# Inflammatory monocytes promote pyogranuloma formation to counteract *Yersinia* blockade of host defense

Daniel Sorobetea[1,2], Rina Matsuda[1,2], Stefan T. Peterson[1], James P. Grayczyk[1], Indira Rao[1], Elise Krespan[1], Matthew Lanza[1], Charles-Antoine Assenmacher[1], Daniel Beiting[1], Enrico Radaelli[1] & Igor Brodsky[1]*

*e-mail: ibrodsky@vet.upenn.edu

Affiliations

1. Department of Pathobiology, School of Veterinary Medicine, University of Pennsylvania, Philadelphia, USA

2. These authors contributed equally

**Abstract**

Granulomas are organized immune cell aggregates that form in response to chronic infection or antigen persistence. *Yersinia pseudotuberculosis* (*Yp*) blocks innate inflammatory signaling and phagocytosis, inducing formation of neutrophil-rich pyogranulomas within lymphoid tissues. Here, we uncover that *Yp* triggers pyogranuloma formation within the murine intestinal mucosa, a site not known to contain such structures. Mice lacking circulating monocytes fail to form defined pyogranulomas, have defects in neutrophil activation, and succumb to *Yp* infection. *Yersinia* lacking the virulence factors that block phagocytosis did not induce pyogranulomas, indicating that intestinal pyogranulomas form in response to *Yp* disruption of phagocytosis. Notably, mutation of a single anti-phagocytic virulence factor, YopH, restored pyogranuloma formation and control of *Yp* infection in monocyte-deficient mice, demonstrating that monocytes override YopH-dependent blockade of innate immune defense. This work reveals an unappreciated site of *Yersinia* intestinal invasion, and defines host and pathogen drivers of intestinal granuloma formation.

## Introduction

Microbial pathogens utilize diverse mechanisms to subvert host immunity in order to replicate and spread to new hosts. While acute infections can be cleared rapidly by the immune system, some pathogens evade immune defenses to cause chronic disease. Inability to clear an infection often results in an alternative strategy of containment within structures termed granulomas to limit pathogen dissemination and tissue damage[1]. Granulomas are characterized by the presence of activated phagocytes, notably monocytes and macrophages, and form in response to a wide variety of infectious organisms[2]. Monocytes are rapidly recruited to infected tissues where they produce inflammatory cytokines and anti-microbial effector molecules, contributing to clearance of multiple pathogens[3–8]. Some pathogens, however, exploit monocytes as a means of dissemination, including *Salmonella enterica*, *Yersinia pestis,* and *Mycobacterium* species[9–12]. The pathogen-specific signals that induce granuloma formation remain poorly defined, raising questions about the precise bacterial and host factors that mediate granuloma formation.

The enteropathogenic *Yersinia, Y. pseudotuberculosis* (*Yp*) and *Y. enterocolitica* (*Ye*), cause self-limiting gastroenteritis and mesenteric lymphadenopathy following enteric infection[13,14]. In immune-compromised patients, bacteria can disseminate systemically to cause a fatal plague-like disease, indicating that the intestinal immune system is critical for control of acute infection. Indeed, studies in mice demonstrate that the intestinal compartment constitutes a major bottleneck against *Yersinia* dissemination, and that bacteria in systemic organs originate predominantly from the intestine rather than gut-associated lymphoid tissues such as the mesenteric lymph nodes (MLN)[15]. A hallmark of *Yersinia* infections is the presence of chronic inflammatory lesions in lymphoid tissue, termed

54 pyogranulomas (PG)[16,18,22]. Like classical granulomas, pyogranulomas are
55 characterized by nodular infiltrates of activated phagocytes, including monocytes and
56 macrophages. Pyogranulomas in particular also contain a core of activated
57 neutrophils. How these structures form and which cell types are required for this
58 process are not known. Notably, the contribution of monocytes to pyogranuloma
59 formation and their role in *Yersinia* restriction are unclear[17,18]. Interestingly,
60 pyogranulomas have been observed in the human intestine in response to both *Yp*
61 and *Ye* infection[14,16,19–21] but have not been observed in murine infection models.
62 Here we identify the formation of pyogranulomas in the murine intestinal
63 mucosa during acute enteric *Yersinia* infection. These lesions are enriched in
64 neutrophils and inflammatory monocytes, and contain comparable numbers of live
65 bacteria to Peyer's patches (PP). Notably, CCR2-deficient mice, which are deficient
66 in circulating inflammatory monocytes[37,38], fail to form defined PG, are unable to
67 contain bacteria within the lesions, and succumb rapidly to infection. Moreover, we
68 find that mice lacking CCR2 exhibit reduced levels of IL-1 cytokines and blunted
69 neutrophil activation within intestinal pyogranulomas. Critically, *Yp* lacking either the
70 virulence plasmid itself, which encodes the type III secreted *Yersinia* Outer Proteins
71 (Yops) present in pathogenic *Yersinia*, or lacking the Yops that block phagocytosis,
72 do not induce detectable pyogranulomas, indicating that pyogranulomas are
73 triggered by *Yersinia* blockade of phagocytosis. Moreover, bacterial restriction and
74 formation of defined granulomatous lesions in CCR2-deficient mice is restored in
75 infections with a YopH mutant unable to block phagocytosis, indicating that
76 inflammatory monocytes enable the host immune system to overcome *Yersinia*
77 blockade of phagocytosis. Altogether, our study identifies an unappreciated site of
78 *Yersinia* colonization within the murine intestinal mucosa, and reveals an essential

79 function for inflammatory monocytes in establishing pyogranuloma architecture that

80 enables *Yersinia* clearance.

## Results

*Intestinal pyogranulomas form acutely following oral Yersinia infection*

*Yersinia pseudotuberculosis* colonizes gut-associated lymphoid tissues, resulting in pyogranuloma formation within five days following oral infection[22]. Interactions between *Yersinia* and immune cells within systemic tissues have been extensively documented[23–25]. In our efforts to investigate the interaction between *Yp* and the intestinal immune system, we observed numerous nodular lesions in the gastrointestinal tract five days post-infection, which appeared as punctate areas of increased opacity along the length of the intestine (Fig. 1a). The total number of lesions in any individual mouse ranged from two to over forty, with a mean of twenty (Extended Data Fig. 1a). Intestinal lesions also formed in response to *Ye* infection (Extended Data Fig. 1a), indicating that these lesions are a conserved response to enteric *Yersinia* infection. The lesions were non-uniformly distributed along the intestinal tract, and were over-represented in the jejunum and ileum (Extended Data Fig. 1b). Histologic analysis of *Yp*-infected intestines revealed focal regions of inflammation characterized by crypt hyperplasia, edema, and submucosal to transmural cellular infiltration, which contrasted with non-lesional areas of the infected intestine that appeared largely unaffected, similar to uninfected controls (Fig. 1b). Furthermore, the lesions contained infiltrates of macrophages and neutrophils surrounding colonies of coccobacilli, similar to structures we and others have observed in lymphoid tissues[22,26], and were therefore termed pyogranulomas (Fig. 1c). Consistently, flow-cytometric analysis of intestinal punch biopsies containing pyogranulomas (PG+), adjacent non-granulomatous tissue (PG-), and uninfected control tissue (uninf) revealed that neutrophils were the most enriched cell type specifically within PG+ tissue, followed by macrophages and inflammatory

106 monocytes (Fig. 1d, Extended Data Fig. 1c). Only minor changes were observed in
107 the frequency or number of eosinophils, dendritic cells, B cells, and T cells in PG+
108 compared to PG- or uninfected tissue (Extended Data Fig. 1d).

109 *Yp* pyogranulomas in lymphoid tissues consist of a central bacterial colony,
110 surrounded proximally by neutrophils, bordered in turn by monocytes and
111 macrophages[18,26]. Similarly, confocal microscopy of whole mount PG+ samples
112 demonstrated that intestinal pyogranulomas also contained a central *Yp* colony
113 surrounded by a dense population of Ly-6G$^{+}$ neutrophils (Fig. 1e). Interestingly, in
114 contrast to pyogranuloma architecture in lymphoid tissues, CCR2$^{+}$ monocytes and
115 macrophages formed a dense mesh-like network of cells that both overlapped with
116 and bordered the neutrophils (Fig. 1e). Consistent with the presence of bacterial
117 colonies detected by histology and fluorescence microscopy, PG+ tissue harbored
118 high numbers of viable bacteria, in contrast to neighboring PG- tissue (Fig. 1f).
119 Moreover, the total bacterial burden in PG+ tissue was equivalent to that found in the
120 PP (Fig. 1g). Since Peyer's patches are viewed as the main entry point and
121 replicative niche for enteropathogenic *Yersinia* following oral innoculation[27,28], our
122 data demonstrate that intestinal pyogranulomas represent a previously
123 unappreciated location of *Yersinia* invasion within the intestinal mucosa, and a likely
124 site of bacterial restriction or potential dissemination[29,30]. Together, these findings
125 uncover a novel site of pyogranulomas that contain high numbers of viable bacteria
126 within the intestinal mucosa, and may serve as an intestinal niche for enteric
127 *Yersinia*.

128

129 *The intestinal innate inflammatory response to* Yersinia *is localized to*
130 *pyogranulomas*

131 Intestinal pyogranulomas represent an unrecognized site for enteric *Yersinia*
132 to interact with the murine mucosal immune system. To define the PG-specific
133 inflammatory response, we performed RNA sequencing of punch biopsies containing
134 pyogranulomas (PG+), adjacent non-pyogranuloma tissue (PG-), and uninfected
135 control tissue. Principal-component analysis showed distinct clustering by sample
136 type (Fig. 2a), and comparison of PG+ and PG- samples revealed 355 upregulated
137 and 363 downregulated genes (Fig. 2b). Top upregulated genes included
138 granulocyte- and monocyte-recruiting chemokines (*Cxcl1, Cxcl2, Cxcl3, Cxcl5*), pro-
139 inflammatory cytokines (*Il1b, Il22*), antimicrobial metal-sequestration proteins
140 (*S100a8, S100a9*), and matrix metalloproteases (*Mmp3*) (Fig. 2c). Gene ontology
141 analysis revealed that chemotaxis of myeloid cells and defense against bacterial
142 pathogens predominated the top upregulated responses within PG+ biopsies (Fig.
143 2d, Extended Data Table 1). These features of the transcriptional response were
144 strikingly similar to those previously reported in *Yp*-infected PP[31]. Indeed, gene set-
145 enrichment analysis indicated that the reported top 50 upregulated genes in *Yp*-
146 infected PP were also enriched in PG+ samples (Fig. 2e). Consistently, protein levels
147 of pro-inflammatory cytokines TNF, CCL2, IL-1β, IL-1α, and IL-6 were elevated
148 within PG+ biopsies compared to PG- and uninfected biopsies (Fig. 2f). Consistent
149 with the histology and microscopy analyses, the inflammatory transcriptional
150 response was localized to PG+ tissue, as PG- samples did not exhibit enrichment of
151 genes or ontology terms related to myeloid cell migration or innate immune-cell
152 activation (Extended Data Fig. 2, Extended Data Table 2). Likewise, production of
153 pro-inflammatory cytokines was not detected above uninfected levels in PG- tissue
154 (Fig. 2e). Altogether, our transcriptional and cytokine analyses indicate that the pro-

155 inflammatory response to *Yp* infection in the gut mucosa is driven by innate immune
156 cells and spatially restricted to pyogranulomas.
157
158 *Inflammatory monocytes are required for organized pyogranuloma formation and*
159 *restriction of Yersinia within intestinal tissue*
160 Inflammatory monocytes promote host defense by differentiating into
161 phagocytes and antigen presenting cells[3,5,7,32,33], producing pro-inflammatory
162 cytokines and antimicrobial molecules[4], and modulating the function of other immune
163 cells to promote pathogen clearance or prevent immunopathology[6,34]. However,
164 monocyte-derived cells can also promote pathogen replication or pathogen
165 dissemination to new infection sites[9,29,30,35,36]. Mice lacking the chemokine receptor
166 CCR2 have a ten-fold reduction in circulating monocytes due to defective bone
167 marrow-egress[37,38]. Monocytes are rapidly recruited to intestinal pyogranulomas (Fig.
168 1) and systemic *Yp* infection sites[18,22,26,39,40]. CCR2-deficiency was reported to be
169 associated with more rapid bacterial clearance from the MLN following enteric
170 infection[18], but increased susceptibility to intravenous *Yp* infection[17]. We therefore
171 sought to dissect the contribution of inflammatory monocytes to anti-*Yersinia* innate
172 immune defense and formation of pyogranulomas. Although infection of CCR2-
173 deficient mice[41,42] resulted in similar numbers of macroscopic intestinal lesions to WT
174 mice (Fig. 3a, Extended Data Fig. 3a), blinded analysis by a board-certified
175 pathologist revealed that intestinal lesions in *Ccr2*$^{gfp/gfp}$ mice (in which insertion of
176 EGFP into the translation initiation site of *Ccr2* disrupts its expression) had a
177 disorganized appearance, and many showed a central region of caseation containing
178 substantial tissue necrosis that was not observed in intestinal PG of WT mice (Fig.
179 3b). Whereas WT pyogranulomas exhibited robust inflammatory infiltrates and a

180 defined cellular organization encapsulating central bacterial colonies, *Ccr2*$^{gfp/gfp}$
181 intestinal lesions contained extensively distributed bacterial colonies with limited
182 inflammatory immune cell recruitment (Fig. 3c). Two independent lines of CCR2-
183 deficient mice had significantly higher bacterial burdens in both PG+ and PG-
184 intestinal tissue biopsies than corresponding tissues of WT mice, suggesting that
185 monocytes restrict enteric *Yp* infection within pyogranulomas and limit dissemination
186 to surrounding intestinal tissue (Fig. 3d, Extended Data Fig. 3b). Consistent with their
187 reduced cellularity in histologic analyses, flow cytometry of *Ccr2*$^{gfp/gfp}$ lesions
188 revealed an overall decrease in viable CD45$^{+}$ hematopoietic cells compared to WT
189 pyogranulomas (Fig. 3e). Consistent with the known role of CCR2 in egress of
190 monocytes out of bone marrow and into circulation[37,38], *Ccr2*$^{gfp/gfp}$ intestinal lesions
191 contained significantly lower numbers of monocytes and macrophages compared
192 with pyogranulomas from WT mice. Surprisingly, despite similar frequencies of
193 neutrophils in the MLN and spleen upon infection (Extended Data Fig. 3c), *Ccr2*$^{gfp/gfp}$
194 intestinal lesions showed reduced neutrophil numbers (Fig. 3e), suggesting that
195 monocytes or monocyte-derived cells promote recruitment, retention, or survival of
196 neutrophils within intestinal pyogranulomas during *Yp* infection. Notably,
197 immunofluorescence microscopy of the lesions revealed that the bacteria expanded
198 outside range of the neutrophil marker Ly-6G, suggesting that neutrophils were
199 unable to effectively contain *Yp* in the absence of monocytes. In contrast, *Yp* was
200 fully encapsulated by neutrophils and CCR2$^{+}$ cells in CCR2-sufficient PGs (Fig. 3f).
201 Intriguingly, neutrophil surface expression of the integrin CD11b, an established
202 marker of neutrophil activation[43–46], was also significantly reduced in both *Ccr2*$^{gfp/gfp}$
203 PGs and MLN compared to WT mice (Fig. 3g, Extended Data Fig. 3d), indicating a
204 defect in neutrophil activation in these tissues in the absence of monocytes.

205 Moreover, IL-1α and IL-1β levels were significantly decreased in *Ccr2*$^{gfp/gfp}$ PGs (Fig.
206 3h), suggesting that monocytes or monocyte-derived cells were required to either
207 directly release IL-1 or promote IL-1 production by other cells within intestinal PGs.
208 CCR2-deficiency specifically impacted IL-1 levels within PGs, as levels of other pro-
209 inflammatory cytokines was not altered in CCR2-deficient mice (Extended Data Fig.
210 3e). Importantly, we found no effect of CCR2 deficiency on CD4$^{+}$ or CD8$^{+}$ T cell
211 numbers[47] in *Ccr2*$^{gfp/gfp}$ intestinal PGs, suggesting that the defect in enteric control of
212 *Yp* in CCR2-defficient mice was not due an effect on T cell numbers (Extended Data
213 Fig. 3f). Altogether, these results demonstrate that monocyte-derived cells are
214 required to establish robust, functional granulomas that limit intestinal bacterial
215 replication and dissemination.
216
217 *Inflammatory monocytes are required for systemic control of Yersinia and host*
218 *survival*
219 Following dissemination from the intestine, *Yp* colonizes and induces PG
220 formation in lymphoid tissues[18,22,26]. Critically, CCR2-deficient mice had significantly
221 higher *Yp* burdens in the MLN and systemic organs (Fig. 4a, Extended Data Fig. 3g).
222 Histopathological analysis revealed that similar to intestinal tissues, infected
223 *Ccr2*$^{gfp/gfp}$ spleens lacked defined pyogranulomas and exhibited widespread tissue
224 necrosis, free bacterial colonies, and sparse immune cell recruitment, which
225 contrasted with WT spleens that contained neutrophils and monocytes that
226 effectively surrounded *Yp* microcolonies (Fig. 4b-c). Notably, mice lacking CCR2
227 succumbed rapidly to acute infection (Fig. 4d, Extended Data Fig. 3h). Importantly,
228 infection of co-housed littermate progeny from heterozygous mating demonstrated
229 that *Ccr2*$^{+/+}$ and *Ccr2*$^{gfp/+}$ mice were equally resistant to *Yp* infection while *Ccr2*$^{gfp/gfp}$

230 littermates succumbed (Fig. 4e), indicating that differences in intestinal microbiota
231 between *Ccr2*$^{gfp/gfp}$ and WT mice were unlikely to account for differences in
232 susceptibility to *Yp* infection. Collectively, our findings demonstrate that inflammatory
233 monocytes are required for formation of organized pyogranulomas in host tissues,
234 thereby limiting tissue necrosis and systemic bacterial dissemination, ultimately
235 enabling bacterial control and host survival following oral *Yp* infection.
236
237 *Intestinal pyogranulomas form in response to Yersinia virulence*
238 Mammalian pathogenic *Yersinia* inject their target cells with effector proteins
239 (Yops) that are encoded on a virulence plasmid (pYV)[48]. Yops block antimicrobial
240 defenses, including phagocytosis, production of reactive oxygen species (ROS), and
241 degranulation[24,49–52]. *Yp* lacking the virulence plasmid (pYV-) are still able to colonize
242 gut-associated lymphoid tissues, including the MLN, during the acute phase of
243 infection without causing disease[53]. As granuloma formation occurs in response to
244 pathogens that thwart immune defenses, we hypothesized that formation of intestinal
245 pyogranulomas is triggered by the activity of *Yp* effector proteins. Indeed, even at a
246 ten-fold higher infectious dose, we were unable to detect any macroscopic intestinal
247 lesions at day 5 post-infection with pYV- bacteria (Fig. 5a), despite significant, albeit
248 lower, bacterial burdens in the intestinal mucosa (Fig. 5b). We likewise found lower
249 bacterial burdens within gut-associated and systemic lymphoid tissues of mice
250 infected with pYV- compared to WT bacteria (Fig. 5c). Intriguingly, monocytes were
251 still recruited to both the intestinal mucosa and MLN in response to of pYV- infection,
252 indicating that absence of detectable pyogranulomas was not due to an absolute
253 lack of inflammatory cell infiltration into the tissue of pYV- infected mice (Fig. 5d,e).
254 Notably, however, neutrophil recruitment to the intestine or MLN was absent in

255 response to pYV- infection, demonstrating that neutrophil recruitment or retention in
256 the intestinal tissue is a response to *Yp* virulence activities (Fig. 5d,e).
257 To test whether specific effectors were responsible for triggering
258 pyogranuloma formation, we infected mice with individual or combined mutants of
259 different Yops. Intestinal lesions formed at similar numbers in mice infected with *Yp*
260 lacking either YopM (*ΔyopM*) or deficient in YopJ enzymatic activity ($YopJ^{C172A}$),
261 which block pyrin inflammasome assembly and MAPK signaling[54–60], respectively,
262 suggesting that neither YopM nor YopJ are solely required to trigger pyogranuloma
263 formation (Extended Data Fig. 4a). A critical virulence function contained on the pYV
264 plasmid is disruption of the actin cytoskeleton, leading to blockade of phagocytosis
265 and inhibition of the reactive oxygen burst[24,61–63]. These Yops (E, H, and T), have
266 partially overlapping functions and can compensate for one another in certain
267 settings[62–69]. Notably, *Yp* containing point mutations in each of the key catalytic
268 residues of these Yops ($YopE^{R144A}$, $YopT^{C139A}$, and $YopH^{R409A}$) did not induce
269 intestinal lesions and had burdens similar to pYV- infection (Fig. 5a-c). In contrast,
270 bacteria lacking only YopE (*ΔyopE*) or both YopE and YopT (*yopET*) induced
271 formation of similar numbers of intestinal lesions (Fig. 5a) and had wild-type levels of
272 intestinal colonization (Fig. 5b,c). These data indicate that YopH is sufficient, in the
273 absence of YopE and YopT, to induce pyogranuloma formation. Interestingly,
274 bacteria lacking only YopH enzymatic activity or YopE alone had similar numbers of
275 macroscopic lesions to wild-type-infected mice (Fig. 5a), suggesting that YopH is
276 sufficient, but not absolutely required to trigger pyogranuloma formation. Notably,
277 while bacteria lacking either YopE or YopH alone induced similar numbers of
278 intestinal lesions to wild-type *Yersinia*, bacteria lacking both YopE and YopH
279 (*yopEH*) induced no detectable lesions, and showed similar levels of colonization to

280 *yopETH* bacteria (Fig. 5a-c). Altogether, these data indicate that intestinal
281 pyogranuloma formation occurs in response to *Yersinia* disruption of host actin
282 cytoskeletal dynamics and is primarily driven by YopE and YopH.
283
284 *Yp restriction by CCR2-deficient mice is restored in absence of YopH activity*
285 Our results demonstrate that YopH is sufficient, but not strictly necessary to
286 induce formation of intestinal pyogranulomas. YopH potently blocks phagocytosis by
287 innate immune cells, including macrophages and neutrophils[24,49,50,62,69,70]. YopH-
288 deficient *Yp* therefore have enhanced susceptibility to neutrophil killing *in vitro* and
289 are attenuated *in vivo*[71–73]. While YopH potently blocks neutrophil functions,
290 neutrophil depletion increases susceptibility to *Yp* and restores virulence to *yopH*-
291 mutant bacteria[50,70], indicating that neutrophil defenses nevertheless counteract
292 YopH activity *in vivo*. How neutrophils counteract the activity of YopH is not
293 understood. Monocyte and neutrophil crosstalk is essential for optimal immune
294 defense in many infectious contexts[74]. However, whether monocytes are required to
295 combat YopH-dependent blockade of neutrophil function is unknown. To test this
296 possibility, we infected CCR2-deficient mice with WT or YopH-mutant *Yp*. Strikingly,
297 CCR2-deficient mice infected with YopH$^{R409A}$ bacteria exhibited robust neutrophil
298 recruitment and containment of bacterial colonies similar to WT mice, in contrast to
299 CCR2-deficient mice infected with WT *Yp* (Fig. 6a). Moreover, both *Ccr2*$^{gfp/gfp}$ and
300 *Ccr2*$^{-/-}$ mice restricted YopH$^{R409A}$ bacteria within the intestine (Fig. 6b, Extended Data
301 Fig. 4a) and systemically (Fig. 6c, Extended Data Fig. 4b). While CCR2-deficient
302 mice rapidly succumbed to WT *Yp*, they survived infection with YopH$^{R409A}$ bacteria
303 similarly to WT mice (Extended Data Fig. 4c). Altogether, our results uncover a key
304 role for monocytes in establishment and function of intestinal pyogranulomas,

305 revealing monocytes as essential in overcoming *Yersinia* suppression of neutrophil

306 function *in vivo* and preventing acute mortality.

307 **Discussion**

308 Granulomas are a conserved immunological response to persistent or long-
309 term infectious and non-infectious stimuli[1,2]. The natural rodent and human pathogen
310 *Yersinia pseudotuberculosis* induces formation of neutrophil-rich lesions termed
311 pyogranulomas in infected lymphoid tissues[14,16]. Here, we report that pyogranulomas
312 form throughout the intestine during murine enteropathogenic *Yersinia* infection.
313 Peyer's patches are considered the primary site of intestinal infection by *Yersinia*.
314 However, intestinal pyogranulomas harbored a similar total bacterial burden as the
315 PPs, suggesting that PGs are a previously unrecognized niche for enteropathogenic
316 *Yersinia* intestinal colonization. Notably, wild-type mice almost entirely restricted
317 intestinal *Yp* and inflammation to these granulomatous foci. The pro-inflammatory
318 transcriptional profile of PGs was similar to *Yp*-infected Peyer's patches[31],
319 suggesting a shared response to intestinal *Yp* infection driven by the recruitment and
320 activation of innate immune cells. These structures may therefore serve to limit
321 bacterial spread and tissue damage within the gut mucosa.

322 We found that monocyte-derived cells were critical for the architectural
323 integrity of PGs in the intestine and deeper tissues during *Yersinia* infection. While
324 other cell types express CCR2, notably activated T cells, we did not observe altered
325 numbers of these cells within intestinal PGs in CCR2-deficient mice. Absence of
326 circulating monocytes was associated with widespread tissue necrosis and elevated
327 bacterial burdens in intestinal and systemic tissues, indicating that the monocyte
328 lineage is critical for containment of *Yersinia* infection. Furthermore, CCR2-
329 deficiency was associated with defective pro-inflammatory IL-1 production and
330 neutrophil activation within intestinal PGs.

331 A previous study reported that monocytes were dispensable for acute control
332 of *Yp* following oral inoculation[18]. These studies employed a distinct *Ccr2*$^{-/-}$ mouse
333 line[32,38], originally generated on the 129 mouse background and backcrossed to
334 C57BL/6[37], raising the possibility that distinct polymorphisms in this mouse line might
335 account for this difference. *Ccr2*$^{gfp/gfp}$ mice were generated on the C57BL/6J
336 background[41], making it unlikely that our findings are due to immunologically
337 impactful polymorphisms that co-segregate with the *Ccr2* locus. Infection of co-
338 housed littermates also demonstrated that increased susceptibility of CCR2-deficient
339 mice is not due to differences in maternally-transmitted or environmentally-acquired
340 intestinal microbiota.
341 Formation of intestinal PGs also required the anti-phagocytic Yops. While
342 combined deficiency in two effector proteins that block phagocytosis, Yops E and H,
343 abrogated PG formation, either effector alone was sufficient to induce PG formation.
344 This suggests that PG formation occurs in response to pathogens that resist immune
345 clearance, and that the anti-phagocytic activities of YopH and YopE independently
346 mediate PG formation. Precisely how blockade of phagocytosis by YopsH and E
347 lead to recruitment of phagocytic cells and assembly of pyogranulomas remains to
348 be determined in future studies.
349 Monocytes and neutrophils comprise a large proportion of Yop-injected
350 cells *in vivo*[75]. YopH blocks neutrophil degranulation, ROS production, phagocytosis,
351 and release of neutrophil extracellular traps[24,50,70,73,76]. Notably, while monocytes
352 were required for host survival in response to WT bacteria, they were dispensable for
353 control of *Yp* lacking YopH activity. Our findings imply that monocytes are critical for
354 host defense against pathogen blockade of neutrophil function, either by directly
355 restricting bacterial growth or enhancing neutrophil-mediated bacterial control.

356 Indeed, intestinal PGs in CCR2-deficient mice exhibited decreased neutrophil
357 numbers and activation, suggesting that monocytes promote neutrophil function
358 during intestinal *Yp* infection. Altogether, our study reveals an unappreciated site of
359 *Yersinia*-host interaction within the intestine, and provides insight into mechanisms of
360 *Yersinia* granuloma formation and function.

361 **Methods**

362 *Animals*

363 C57BL/6 wild-type and *Ccr2*$^{gfp/gfp}$ mice[41] (in which insertion of EGFP into the
364 translation initiation site of *Ccr2* disrupts its expression) were acquired from the
365 Jackson Laboratory and bred at the University of Pennsylvania. *Ccr2*$^{-/-}$ mice[42] were
366 provided by Dr. Sunny Shin (University of Pennsylvania). Unless specifically noted,
367 all animals were bred by homozygous mating and housed separately by genotype.
368 All animal studies were performed in strict accordance with University of
369 Pennsylvania Institutional Animal Care and Use Committee-approved protocols.

370

371 *Bacteria*

372 Wild-type *Yp* (strain 32777, serogroup O1)[77] and isogenic mutants[58,77–79] were
373 provided by Dr. James Bliska (Dartmouth College). *Ye* (strain 8081, serogroup O8)[80]
374 was provided by Dr. Stanley Falkow (Stanford University). Additional mutants lacking
375 YopE (*ΔyopE*), enzymatic activity of YopH (YopH$^{R409A}$) or YopE/YopT/YopH
376 (YopE$^{R144A}$T$^{C139A}$H$^{R409A}$, denoted *yopETH*) were generated by two-step allelic
377 recombination as previously described[79] with plasmids provided by Dr. James Bliska.
378 Fluorescent *Yp* (mCherry$^{+}$) was generated from plasmids provided by Dr. Kimberly
379 Davis (Johns Hopkins University).

380

381 *Infections*

382 *Yp* and *Ye* were cultured to stationary phase at 28°C and 250 rpm shaking for
383 16 hours in 2xYT broth supplemented with 2 µg/ml triclosan (Millipore Sigma). Mice
384 of either sex between 8-12 weeks of age were fasted for 16 hours and subsequently
385 inoculated by oral gavage with 100-200 µl phosphate-buffered saline (PBS). All

386 bacterial strains were administered at $2x10^8$ colony-forming units (CFU) per mouse
387 with the exception of pYV- which was administered at $20x10^8$ CFU per mouse.
388
389 *Bacterial CFU quantifications*
390 In order to determine bacterial burdens, tissue biopsies were collected in
391 sterile PBS, weighed, homogenized for 40 seconds with 6.35 mm ceramic spheres
392 (MP Biomedical) using a FastPrep-24 bead beater (MP Biomedical) and serially
393 diluted tenfold in PBS before being plated on LB agar supplemented with 2 µg/ml
394 triclosan and incubated for two days at room temperature. Dilutions of each sample
395 were plated in triplicate and expressed as the mean CFU per gram of tissue or per
396 biopsy.
397
398 *Protein quantifications*
399 Cytokines were measured in supernatants from homogenized tissue using
400 Cytometric Bead Array (BD Biosciences) according to manufacturer's instructions
401 with the following modification: the amount of capture beads, detection reagents, and
402 sample volumes was scaled down tenfold. Data were collected on an LSRFortessa
403 flow cytometer (BD Biosciences) and analyzed with FlowJo v10 (BD Biosciences).
404
405 *Tissue preparation and cell isolation*
406 Lymph nodes were homogenized in R10 buffer consisting of RPMI 1640
407 (Millipore Sigma) supplemented with 10 mM HEPES (Millipore Sigma), 10% fetal
408 bovine serum (Omega Scientific), 1 mM sodium pyruvate (Thermo-Fisher Scientific)
409 and 100 U/ml penicillin + 100 µg/ml streptomycin (Thermo Fisher Scientific), then
410 passed through 70 µm cell strainers (Fisher Scientific). Intestines were excised,

411 flushed luminally with sterile PBS to remove the feces, opened longitudinally along
412 the mesenteric side and placed luminal side down on cutting boards (Epicurean).
413 Small-intestinal tissue containing pyogranulomas (PG+), adjacent non-
414 granulomatous areas (PG-) and uninfected control tissue (uninf) were excised using
415 a 2 mm-ø dermal punch-biopsy tool (Keyes). Biopsies within each mouse were
416 pooled groupwise, suspended in epithelial-dissociation buffer consisting of calcium
417 and magnesium-free HBSS (Thermo Fisher Scientific) supplemented with 15 mM
418 HEPES, 10 mg/ml bovine serum albumin (Millipore Sigma), 5 mM EDTA and 100
419 U/ml penicillin + 100 µg/ml streptomycin, then incubated for 30 minutes at 37°C
420 under continuous agitation. To isolate immune cells from the lamina propria, the
421 tissue was enzymatically digested in R10 buffer, along with 0.5 Wünsch units/ml
422 liberase TM (Roche), 30 µg/ml DNase I (Roche), and 5 mM $CaCl_2$ for 20 min at 37°C
423 under continuous agitation. The resulting cell suspensions were filtered through 100
424 µm cell strainers (Fisher Scientific) and subjected to density-gradient centrifugation
425 using Percoll (GE Healthcare). Briefly, cells were suspended in 40% Percoll and
426 centrifuged over a 70% Percoll layer for 20 min at 600 × g with lowest brake at room
427 temperature. Cells collected between the layers were washed with R10 for
428 downstream analysis.
429
430 *Flow cytometry*
431 Unspecific Fc binding was blocked for 15 minutes on ice with unconjugated
432 anti-CD16/CD32 (clone 93; Thermo-Fisher Scientific). Cells were subsequently
433 fluorescently labeled for 30 minutes on ice with the following antibodies and
434 reagents: PE-conjugated rat anti-mouse Siglec-F (E50-2440; BD Biosciences), PE-
435 TxR-conjugated rat anti-mouse CD11b (M1/70.15; Thermo Fisher Scientific), PE-

436 Cy5-conjugated mouse anti-mouse NK1.1 (PK136; BioLegend), PE-Cy5.5-
437 conjugated rat anti-mouse CD4 (RM4-5; Thermo Fisher Scientific), PE-Cy7-
438 conjugated rat anti-mouse CD3 (17A2; BioLegend), FITC-conjugated Armenian
439 hamster anti-mouse CD11c (N418; BioLegend), PerCP-Cy5.5-conjugated rat anti-
440 mouse Ly-6C (HK1.4; Thermo Fisher Scientific), PB-conjugated rat anti-mouse
441 CD90.2 (53-2.1; BioLegend), BV510-conjugated rat anti-mouse CD19 (1D3; BD
442 Biosciences), BV605-conjugated Armenian hamster anti-mouse TCRβ (H57-597; BD
443 Biosciences), BV650-conjugated rat anti-mouse I-A/I-E (M5/114.15.2; BD
444 Biosciences), BV711-conjugated rat anti-mouse CD8α (53-6.7; BD Biosciences),
445 BV785-conjugated rat anti-mouse Ly-6G (1A8; Thermo Fisher Scientific), AF647-
446 conjugated mouse anti-mouse CD64 (X54-5/7.1; BD Biosciences) and AF700-
447 conjugated mouse anti-mouse CD45.2 (104; BioLegend) along with eF780 viability
448 dye (BioLegend) diluted in PBS according to manufacturer's instructions. Cells were
449 fixed for 20 minutes on ice with Cytofix/Cytoperm Fixation/Permeabilization solution
450 (BD Biosciences). Cells were acquired on an LSRFortessa flow cytometer and data
451 was analyzed with FlowJo v10. Dead and clustered cells were removed from all
452 analyses.
453
454 *Histology*
455 Tissues were fixed in 10% neutral-buffered formalin (Fisher Scientific) and
456 stored at 4°C until further processed. Tissue pieces were embedded in paraffin,
457 sectioned by standard histological techniques and stained with hematoxylin and
458 eosin for subsequent histopathological disease scoring by blinded board-certified
459 pathologists. Tissue sections were given scores between 0-4 (healthy-severe) for
460 multiple parameters, including degree of inflammatory cell infiltration, necrosis, and

461 free bacterial colonies along with tissue-specific parameters such as villus blunting
462 and crypt hyperplasia. Healthy mice were characterized by and subsequently scored
463 as having none or low levels of the parameters described, whereas severely afflicted
464 mice presented with high amounts of the respective parameters.
465
466 *Fluorescence microscopy*
467 Small-intestinal tissue was dissected and luminal contents were flushed out
468 with PBS. Intestines were opened longitudinally and ~0.5 cm tissue pieces
469 containing macroscopically visible lesions were excised. Tissues were fixed in 1%
470 paraformaldehyde overnight then blocked for two hours at room temperature in
471 blocking solution containing 10% BSA, 1 µg/ml anti-CD16/32, and 0.5% normal rat
472 IgG in PBS. AF647-conjugated anti-Ly-6G antibody (1A8; Biolegend) was added at
473 0.01 mg/ml in 100 µl PBS per sample, then whole tissue was stained for 24 hours at
474 4°C. Samples were washed three times with PBS, mounted whole onto slides in
475 Prolong Glass Antifade Mountant (Thermo Fisher Scientific) and cured for two days
476 at room temperature. Images were acquired on a DMI 6000 laser-scanning confocal
477 microscope (Leica) with a 20x NA 0.75 oil-immersion objective. The center of the
478 sample was determined in the Z direction, then imaged. Images were analyzed using
479 ImageJ v2.1.
480
481 *RNA sequencing*
482 Intestinal punch biopsies were collected as described above. Five biopsies
483 per sample type were pooled for each mouse. RNA was extracted using the RNeasy
484 Plus Mini Kit (Qiagen). Sequence-ready libraries were prepared using the Illumina
485 TruSeq Stranded Total RNA kit with Ribo-Zero Gold rRNA depletion (Illumina).

486 Quality assessment and quantification of RNA preparations and libraries were
487 carried out using an Agilent 4200 TapeStation and Qubit 3, respectively. Samples
488 were sequenced on an Illumina NextSeq 500 to produce 150–base pair single end
489 reads with a mean sequencing depth of 9 million reads per sample. Raw reads from
490 this study were mapped to the mouse reference transcriptome (Ensembl; Mus
491 musculus GRCm38) using Kallisto v0.46.2[81]. Raw sequence data are available on
492 the Gene Expression Omnibus (GEO; accession no. GSE194334).
493 All subsequent analyses were carried out using the statistical computing
494 environment R v4.0.3 in RStudio v1.2.5042 and Bioconductor[82]. Briefly, transcript
495 quantification data were summarized to genes using the tximport package[83] and
496 normalized using the trimmed mean of M values (TMM) method in edgeR[84]. Genes
497 with <1 CPM in 3 samples were filtered out. Normalized filtered data were variance-
498 stabilized using the voom function in limma[85], and differentially expressed genes
499 were identified with linear modeling using limma (FDR ≤ 0.05; absolute $\log_2$FC ≥ 1)
500 after correcting for multiple testing using Benjamini-Hochberg.
501
502 *Statistics*
503 Statistical analyses were performed using Prism v9.0 (GraphPad Software).
504 Independent groups were compared by Mann-Whitney U test. Survival curves were
505 compared by Mantel-Cox test. Statistical significance is denoted * ($p<0.05$), **
506 ($p<0.01$), *** ($p<0.001$), **** ($p<0.0001$), NS (not significant).

507 **References**


508 1. Pagán, A. J. & Ramakrishnan, L. The Formation and Function of Granulomas.
509 *Annu. Rev. Immunol.* **36**, 639–665 (2018).
510 2. Petersen, H. J. & Smith, A. M. The Role of the Innate Immune System in
511 Granulomatous Disorders. *Front. Immunol.* **4**, 1–11 (2013).
512 3. Serbina, N. V, Salazar-Mather, T. P., Biron, C. A., Kuziel, W. A. & Pamer, E.
513 G. TNF/iNOS-producing dendritic cells mediate innate immune defense
514 against bacterial infection. *Immunity* **19**, 59–70 (2003).
515 4. Casson, C. N. *et al.* Neutrophils and Ly6Chi monocytes collaborate in
516 generating an optimal cytokine response that protects against pulmonary
517 Legionella pneumophila infection. *PLoS Pathog.* **13**, e1006309 (2017).
518 5. Dunay, I. R. *et al.* Gr1+ Inflammatory Monocytes Are Required for Mucosal
519 Resistance to the Pathogen Toxoplasma gondii. *Immunity* **29**, 306–317 (2008).
520 6. Espinosa, V. *et al.* Inflammatory Monocytes Orchestrate Innate Antifungal
521 Immunity in the Lung. *PLoS Pathog.* **10**, e1003940 (2014).
522 7. Seo, S.-U. *et al.* Intestinal macrophages arising from CCR2+ monocytes
523 control pathogen infection by activating innate lymphoid cells. *Nat. Commun.*
524 **6**, 8010 (2015).
525 8. Petermann, M. *et al.* CCR2 Deficiency Impairs Ly6Clo and Ly6Chi Monocyte
526 Responses in Orientia tsutsugamushi Infection. *Front. Immunol.* **12**, 670219
527 (2021).
528 9. Antonelli, L. R. *et al.* Intranasal Poly-IC treatment exacerbates tuberculosis in
529 mice through the pulmonary recruitment of a pathogen-permissive
530 monocyte/macrophage population. *J. Clin. Invest.* **120**, 1674–1682 (2010).
531 10. St. John, A. L. *et al.* S1P-Dependent Trafficking of Intracellular Yersinia pestis

532 through Lymph nodes establishes buboes and systemic infection. *Immunity* **41**,
533 440–450 (2014).
534 11. Cambier, C. *et al.* Mycobacteria manipulate macrophage recruitment through
535 coordinated use of membrane lipids. *Nature* **505**, 218–222 (2014).
536 12. Eisele, N. A. *et al.* Salmonella require the fatty acid regulator PPARδ for the
537 establishment of a metabolic environment essential for long term persistence.
538 **14**, 171–182 (2013).
539 13. Paff, J. R., Triplett, D. A. & Saari, T. N. Clinical and Laboratory Aspects of
540 Yersinia pseudotuberculosis Infections, with a Report of Two Cases. *Am. J.*
541 *Clin. Pathol.* **66**, 101–110 (1976).
542 14. El-Maraghi, N. R. H. & Mair, N. S. The Histopathology of Enteric Infection with
543 Yersinia pseudotuberculosis. *Am. J. Clin. Pathol.* **71**, 631–639 (1979).
544 15. Barnes, P. D., Bergman, M. A., Mecsas, J. C. & Isberg, R. R. Yersinia
545 pseudotuberculosis disseminates directly from a replicating bacterial pool in
546 the intestine. *J. Exp. Med.* **203**, 1591–601 (2006).
547 16. Lamps, L. W. *et al.* The Role of Yersinia enterocolitica and Yersinia
548 pseudotuberculosis in Granulomatous Appendicitis: A Histologic and Molecular
549 Study. *Am. J. Surg. Pathol.* **25**, 508–515 (2001).
550 17. Zhang, Y., Tam, J. W., Mena, P., van der Velden, A. W. M. & Bliska, J. B.
551 CCR2+ Inflammatory Dendritic Cells and Translocation of Antigen by Type III
552 Secretion Are Required for the Exceptionally Large CD8+ T Cell Response to
553 the Protective YopE69-77 Epitope during Yersinia Infection. *PLoS Pathog.* **11**,
554 e1005167 (2015).
555 18. Zhang, Y., Khairallah, C., Sheridan, B. S., van der Velden, A. W. M. & Bliska,
556 J. B. CCR2+ Inflammatory Monocytes Are Recruited to Yersinia

557 pseudotuberculosis Pyogranulomas and Dictate Adaptive Responses at the
558 Expense of Innate Immunity during Oral Infection. *Infect. Immun.* **86**, e00782-
559 17 (2018).
560 19. Kojima, M. *et al.* Immunohistological findings of suppurative granulomas of
561 Yersinia enterocolitica appendicitis: A report of two cases. *Pathol. Res. Pract.*
562 **203**, 115–119 (2007).
563 20. Rohena, F. J., Almira-Suárez, M. I. & González-Keelan, C. Granulomatous
564 Enterocolitis Secondary to Yersinia in an 11-year-old Boy from Puerto Rico,
565 Confirmed by PCR: A Case Report. *P. R. Health Sci. J.* **33**, 27–30 (2014).
566 21. Richardson, T., Jones, M., Akhtar, Y. & Pollard, J. Suspicious Yersinia
567 granulomatous enterocolitis mimicking appendicitis. *BMJ Case Rep.* bcr-2018-
568 224177 (2018). doi:10.1136/bcr-2018-224177
569 22. Peterson, L. W. *et al.* RIPK1-dependent apoptosis bypasses pathogen
570 blockade of innate signaling to promote immune defense. *J. Exp. Med.* **214**,
571 3171–3182 (2017).
572 23. Tsutomu, U. Studies on the Pathogenicity of Yersinia enterocolitica III.
573 Comparative Studies between Y. enterocolitica and Y. pseudotuberculosis.
574 *Microbiol. Immunol.* **21**, 505–516 (1977).
575 24. Bliska, J. B., Brodsky, I. E. & Mecsas, J. Role of the Yersinia
576 pseudotuberculosis Virulence Plasmid in Pathogen-Phagocyte Interactions in
577 Mesenteric Lymph Nodes. *EcoSal Plus* **9**, eESP-0014-2021 (2021).
578 25. Davis, K. M. All Yersinia Are Not Created Equal: Phenotypic Adaptation to
579 Distinct Niches Within Mammalian Tissues. *Front. Cell. Infect. Microbiol.* **8**, 1–8
580 (2018).
581 26. Davis, K. M., Mohammadi, S. & Isberg, R. R. Community Behavior and Spatial

582 Regulation within a Bacterial Microcolony in Deep Tissue Sites Serves to
583 Protect against Host Attack. *Cell Host Microbe* **17**, 21–31 (2015).
584 27. Clark, M. A., Hirst, B. H. & Jepson, M. A. M-cell Surface β1 Integrin Expression
585 and Invasin-Mediated Targeting of Yersinia pseudotuberculosis to Mouse
586 Peyer's Patch M Cells. *Infect. Immun.* **66**, 1237–1243 (1998).
587 28. Fasciano, A. C. *et al.* Yersinia pseudotuberculosis YopE prevents uptake by M
588 cells and instigates M cell extrusion in human ileal enteroid-derived
589 monolayers. *Gut Microbes* **13**, 1988390 (2021).
590 29. Clay, H. *et al.* Dichotomous Role of the Macrophage in Early Mycobacterium
591 marinum Infection of the Zebrafish. *Cell Host Microbe* **2**, 29–39 (2007).
592 30. Davis, J. M. & Ramakrishnan, L. The Role of the Granuloma in Expansion and
593 Dissemination of Early Tuberculous Infection. *Cell* **136**, 37–49 (2009).
594 31. Nuss, A. M. *et al.* Tissue dual RNA-seq allows fast discovery of infection-
595 specific functions and riboregulators shaping host-pathogen transcriptomes.
596 *Proc. Natl. Acad. Sci. U. S. A.* **114**, E791–E800 (2017).
597 32. Zigmond, E. *et al.* Ly6C hi Monocytes in the Inflamed Colon Give Rise to
598 Proinflammatory Effector Cells and Migratory Antigen-Presenting Cells.
599 *Immunity* **37**, 1076–1090 (2012).
600 33. Hohl, T. M. *et al.* Inflammatory Monocytes Facilitate Adaptive CD4 T Cell
601 Responses during Respiratory Fungal Infection. *Cell Host Microbe* **6**, 470–481
602 (2009).
603 34. Grainger, J. R. *et al.* Inflammatory monocytes regulate pathologic responses to
604 commensals during acute gastrointestinal infection. *Nat. Med.* **19**, 713–721
605 (2013).
606 35. Repasy, T. *et al.* Intracellular bacillary burden reflects a burst size for

607 Mycobacterium tuberculosis in vivo. *PLoS Pathog.* **9**, e1003190 (2013).
608 36. Cronan, M. R. *et al.* Macrophage Epithelial Reprogramming Underlies
609 Mycobacterial Granuloma Formation and Promotes Infection. *Immunity* **45**,
610 861–876 (2016).
611 37. Kuziel, W. A. *et al.* Severe reduction in leukocyte adhesion and monocyte
612 extravasation in mice deficient in CC chemokine receptor 2. *Proc. Natl. Acad.*
613 *Sci. U. S. A.* **94**, 12053–12058 (1997).
614 38. Serbina, N. V & Pamer, E. G. Monocyte emigration from bone marrow during
615 bacterial infection requires signals mediated by chemokine receptor CCR2.
616 *Nat. Immunol.* **7**, 311–317 (2006).
617 39. Philip, N. H. *et al.* Caspase-8 mediates caspase-1 processing and innate
618 immune defense in response to bacterial blockade of NF-κB and MAPK
619 signaling. *Proc. Natl. Acad. Sci. U. S. A.* **111**, 7385–7390 (2014).
620 40. Philip, N. H. *et al.* Activity of Uncleaved Caspase-8 Controls Anti-bacterial
621 Immune Defense and TLR-Induced Cytokine Production Independent of Cell
622 Death. *PLoS Pathog.* **12**, e1005910 (2016).
623 41. Satpathy, A. T. *et al.* Notch2-dependent classical dendritic cells orchestrate
624 intestinal immunity to attaching-and-effacing bacterial pathogens. *Nat.*
625 *Immunol.* **14**, 937–948 (2013).
626 42. Boring, L. *et al.* Impaired Monocyte Migration and Reduced Type 1 (Th1)
627 Cytokine Responses in C-C Chemokine Receptor 2 Knockout Mice. *J. Clin.*
628 *Invest.* **100**, 2552–2561 (1997).
629 43. Borjesson, D. L., Simon, S. I., Hodzic, E., Ballantyne, C. M. & Barthold, S. W.
630 Kinetics of CD11b/CD18 Up-Regulation During Infection with the Agent of
631 Human Granulocytic Ehrlichiosis in Mice. *Lab. Investig.* **82**, 303–311 (2002).

632 44. Mann, B. S. & Chung, K. F. Blood neutrophil activation markers in severe
633 asthma: lack of inhibition by prednisolone therapy. *Respir. Res.* **7**, 1–10
634 (2006).
635 45. Yipp, B. G. *et al.* The lung is a host defense niche for immediate neutrophil-
636 mediated vascular protection. *Sci. Immunol.* **2**, eaam8929 (2017).
637 46. Yoon, J. W., Pahl, M. V & Vaziri, N. D. Spontaneous leukocyte activation and
638 oxygen-free radical generation in end-stage renal disease. *Kidney Int.* **71**,
639 167–172 (2007).
640 47. Bakos, E. *et al.* CCR2 Regulates the Immune Response by Modulating the
641 Interconversion and Function of Effector and Regulatory T Cells. *J. Immunol.*
642 **198**, 4659–4671 (2017).
643 48. Portnoy, D. A., Wolf-Watz, H., Bolin, I., Beeder, A. B. & Falkow, S.
644 Characterization of Common Virulence Plasmids in Yersinia Species and Their
645 Role in the Expression of Outer Membrane Proteins. *Infect. Immun.* **43**, 108–
646 114 (1984).
647 49. Zhang, L. *et al.* The Functions of Effector Proteins in Yersinia Virulence. *Polish*
648 *J. Microbiol.* **65**, 5–12 (2016).
649 50. Shaban, L. *et al.* Yersinia pseudotuberculosis YopH targets SKAP2-dependent
650 and independent signaling pathways to block neutrophil antimicrobial
651 mechanisms during infection. *PLOS Pathog.* **16**, e1008576 (2020).
652 51. Green, E. R. *et al.* Fis Is Essential for Yersinia pseudotuberculosis Virulence
653 and Protects against Reactive Oxygen Species Produced by Phagocytic Cells
654 during Infection. *PLoS Pathog.* **12**, e1005898 (2016).
655 52. Songsungthong, W., Higgins, M. C., Rolán, H. G., Murphy, J. L. & Mecsas, J.
656 ROS-inhibitory activity of YopE is required for full virulence of Yersinia in mice.

657 *Cell. Microbiol.* **12**, 988–1001 (2010).
658 53. Balada-Llasat, J. M. & Mecsas, J. C. Yersinia Has a Tropism for B and T Cell
659 Zones of Lymph Nodes That Is Independent of the Type III Secretion System.
660 *PLoS Pathog.* **2**, e86 (2006).
661 54. Yoon, S., Liu, Z., Eyobo, Y. & Orth, K. Yersinia Effector YopJ Inhibits Yeast
662 MAPK Signaling Pathways by an Evolutionarily Conserved Mechanism. *J. Biol.*
663 *Chem.* **278**, 2131–2135 (2003).
664 55. Mukherjee, S. *et al.* Yersinia YopJ Acetylates and Inhibits Kinase Activation by
665 Blocking Phosphorylation. *Science* **312**, 1211–1214 (2006).
666 56. Palmer, L. E., Hobbie, S., Galán, J. E. & Bliska, J. B. YopJ of Yersinia
667 pseudotuberculosis is required for the inhibition of macrophage TNF-α
668 production and downregulation of the MAP kinases p38 and JNK. *Mol.*
669 *Microbiol.* **27**, 953–965 (1998).
670 57. Brodsky, I. E. & Medzhitov, R. Reduced Secretion of YopJ by Yersinia Limits
671 In Vivo Cell Death but Enhances Bacterial Virulence. *PLoS Pathog.* **4**,
672 e1000067 (2008).
673 58. Chung, L. K. *et al.* The Yersinia Virulence Factor YopM Hijacks Host Kinases
674 to Inhibit Type III Effector-Triggered Activation of the Pyrin Inflammasome. *Cell*
675 *Host Microbe* **20**, 296–306 (2016).
676 59. Larock, C. N. & Cookson, B. T. The Yersinia Virulence Effector YopM Binds
677 Caspase-1 to Arrest Inflammasome Assembly and Processing. *Cell Host*
678 *Microbe* **12**, 799–805 (2012).
679 60. Ratner, D. *et al.* The Yersinia pestis Effector YopM Inhibits Pyrin
680 Inflammasome Activation. *PLoS Pathog.* **12**, 1–17 (2016).
681 61. Grosdent, N., Maridonneau-Parini, I., Sory, M.-P. & Cornelis, G. R. Role of

682 Yops and Adhesins in Resistance of Yersinia enterocolitica to Phagocytosis.
683 *Infect. Immun.* **70**, 4165–4176 (2002).
684 62. Green, S. P., Hartland, E. L., M., Robins-Browne, R. M. & Phillips, W. A. Role
685 of YopH in the suppression of tyrosine phosphorylation and respiratory burst
686 activity in murine macrophages infected with Yersinia enterocolitica. *J. Leukoc.*
687 *Biol.* **57**, 972–977 (1995).
688 63. Bliska, J. B. & Black, D. S. Inhibition of the Fc Receptor-Mediated Oxidative
689 Burst in Macrophages by the Yersinia pseudotuberculosis Tyrosine
690 Phosphatase. *Infect. Immun.* **63**, 681–685 (1995).
691 64. Bliska, J. B., Guan, K., Dixon, J. E. & Falkow, S. Tyrosine phosphate
692 hydrolysis of host proteins by an essential Yersinia virulence determinant.
693 *Proc. Natl. Acad. Sci. U. S. A.* **88**, 1187–1191 (1991).
694 65. Rosqvist, R., Bölin, I. & Wolf-Watz, H. Inhibition of Phagocytosis in Yersinia
695 pseudotuberculosis: a Virulence Plasmid-Encoded Ability Involving the Yop2b
696 Protein. *Infect. Immun.* **56**, 2139–2143 (1988).
697 66. Rosqvist, R., Forsberg, Å. & Wolf-Watz, H. Intracellular Targeting of the
698 Yersinia YopE Cytotoxin in Mammalian Cells Induces Actin Microfilament
699 Disruption. *Infect. Immun.* **59**, 4562–4569 (1991).
700 67. Galyov, E. E., Håkansson, S., Forsberg, Å. & Wolf-Watz, H. A secreted protein
701 kinase of Yersinia pseudotuberculosis is an indispensable virulence
702 determinant. *Nature* **361**, 33–50 (1993).
703 68. Black, D. S. & Bliska, J. B. The RhoGAP activity of the Yersinia
704 pseudotuberculosis cytotoxin YopE is required for antiphagocytic function and
705 virulence. *Mol. Microbiol.* **37**, 515–527 (2000).
706 69. Mecsas, J., Raupach, B. & Falkow, S. The Yersinia Yops inhibit invasion of

707 Listeria, Shigella and Edwardsiella but not Salmonella into epithelial cells. *Mol.*
708 *Microbiol.* **28**, 1269–1281 (1998).
709 70. Rolán, H. G., Durand, E. A. & Mecsas, J. Identifying Yersinia YopH-Targeted
710 Signal Transduction Pathways that Impair Neutrophil Responses during In
711 Vivo Murine Infection. *Cell Host Microbe* **14**, 306–317 (2013).
712 71. Logsdon, L. K. & Mecsas, J. C. Requirement of the Yersinia
713 pseudotuberculosis Effectors YopH and YopE in Colonization and Persistence
714 in Intestinal and Lymph Tissues. *Infect. Immun.* **71**, 4595–4607 (2003).
715 72. Fisher, M. L., Castillo, C. & Mecsas, J. Intranasal Inoculation of Mice with
716 Yersinia pseudotuberculosis Causes a Lethal Lung Infection That Is
717 Dependent on Yersinia Outer Proteins and PhoP. *Infect. Immun.* **75**, 429–442
718 (2007).
719 73. Westermark, L., Fahlgren, A. & Fällman, M. Yersinia pseudotuberculosis
720 Efficiently Escapes Polymorphonuclear Neutrophils during Early Infection.
721 *Infect. Immun.* **82**, 1181–1191 (2014).
722 74. Silva, M. T. When two is better than one: macrophages and neutrophils work in
723 concert in innate immunity as complementary and cooperative partners of a
724 myeloid phagocyte system. *J. Leukoc. Biol.* **87**, 93–106 (2010).
725 75. Durand, E. A., Maldonado-Arocho, F. J., Castillo, C., Walsh, R. L. & Mecsas, J.
726 C. The presence of professional phagocytes dictates the number of host cells
727 targeted for Yop translocation during infection. *Cell. Microbiol.* **12**, 1064–1082
728 (2010).
729 76. Taheri, N., Fahlgren, A. & Fällman, M. Yersinia pseudotuberculosis Blocks
730 Neutrophil Degranulation. *Infect. Immun.* **84**, 3369–3378 (2016).
731 77. Simonet, M. & Falkow, S. Invasin expression in Yersinia pseudotuberculosis.

732 *Infect. Immun.* **60**, 4414–4417 (1992).
733 78. McPhee, J. B., Mena, P. & Bliska, J. B. Delineation of Regions of the Yersinia
734 YopM Protein Required for Interaction with the RSK1 and PRK2 Host Kinases
735 and Their Requirement for Interleukin-10 Production and Virulence. *Infect.*
736 *Immun.* **78**, 3529–3539 (2010).
737 79. Zhang, Y., Murtha, J., Roberts, M. A., Siegel, R. M. & Bliska, J. B. Type III
738 secretion decreases bacterial and host survival following phagocytosis of
739 Yersinia pseudotuberculosis by macrophages. *Infect. Immun.* **76**, 4299–4310
740 (2008).
741 80. Portnoy, D. A., Moseley, S. L. & Falkow, S. Characterization of Plasmids and
742 Plasmid-Associated Determinants of Yersinia enterocolitica Pathogenesis.
743 *Infect. Immun.* **31**, 775–782 (1981).
744 81. Bray, N. L., Pimentel, H., Melsted, P. & Pachter, L. Near-optimal probabilistic
745 RNA-seq quantification. *Nat. Biotechnol.* **34**, 525–527 (2016).
746 82. Huber, W. *et al.* Orchestrating high-throughput genomic analysis with
747 Bioconductor. *Nat. Methods* **12**, 115–121 (2015).
748 83. Soneson, C., Love, M. I. & Robinson, M. D. Differential analyses for RNA-seq:
749 transcript-level estimates improve gene-level inferences. *F1000Research* **4**,
750 1521 (2016).
751 84. Robinson, M. D., McCarthy, D. J. & Smyth, G. K. edgeR: A Bioconductor
752 package for differential expression analysis of digital gene expression data.
753 *Bioinformatics* **26**, 139–140 (2010).
754 85. Ritchie, M. E. *et al.* limma powers differential expression analyses for RNA-
755 sequencing and microarray studies. *Nucleic Acids Res.* **43**, e47 (2015).
756

757 **Acknowledgements**

758 We thank Dr. James Bliska for generously providing plasmids for Yop mutant
759 *Yp* strains, as well as Dr. Kimberly Davis for generously providing the mCherry+ *Yp*
760 plasmid. We thank the staff at the PennVet Comparative Pathology Core for their
761 help in preparing the histological samples. We thank Dr. David Christian and Dr.
762 Andrea Stout for key advice on confocal microscopy methods, and Dr. Sunny Shin
763 for constructive editorial comments and scientific discussion. This work was
764 supported by NIH Awards R01AI128530, R01139102A1 (IEB) and a BWF
765 Investigator in the Pathogenesis of Infectious Disease Award (IEB); the Foundation
766 Blanceflor Postdoctoral Scholarship (DS), the Swedish Society for Medical Research
767 postdoctoral fellowship (DS) and the Sweden-America Foundation J. Sigfrid Edström
768 award (DS); NIH NRSA F31AI160741-01 (RM); Mark Foundation Grant 19-011MIA,
769 and F32 AI164655 (JPG); NSF GRFP Award (SP). We thank members of the
770 Brodsky lab for scientific discussion and Dr. Daniel Grubaugh for comments on the
771 manuscript.

772 **Author contributions**

773 DS established the initial findings of intestinal granulomas. DS, RM, and IEB
774 conceptualized the study and devised experiments. DS and RM devised the
775 methodology and performed experiments. SP, JPG, and IR performed experiments.
776 CAA, ER, and ML performed the histology and histopathological scoring. EK
777 prepared the RNA-sequencing libraries. RM and DB analyzed the RNA-sequencing
778 data. IEB acquired the funding and supervised the study. DS, RM, and IEB wrote the
779 original draft. All authors reviewed and edited the manuscript.

## Competing interests

The author declare no competing interests.

782 **Figure legends**

783 **Figure 1. Intestinal pyogranulomas form acutely following oral *Yersinia***

784 **infection**

785 (**a**) Longitudinal small-intestinal segments from uninf (top) and *Yp*-infected (bottom)

786 mice with arrows depicting lesions. Scale bar = 3 mm. Representative image of >3

787 independent experiments.

788 (**b**) H&E-stained paraffin-embedded longitudinal small-intestinal sections from uninf

789 (left) and *Yp*-infected (middle and right) mice. Scale bars = 200 μm. Representative

790 images of three independent experiments.

791 (**c**) H&E-stained paraffin-embedded longitudinal small-intestinal PG+ section from a

792 *Yp*-infected mouse depicting an encircled bacterial colony. Scale bar = 10 μm.

793 Representative image of three independent experiments.

794 (**d**) Flow-cytometry plots (left side) identifying CD11b$^{+}$ Ly-6G$^{+}$ neutrophils (top),

795 CD11b$^{+}$ CD64$^{+}$ Ly-6C$^{+}$ monocytes, and CD11b$^{+}$ CD64$^{+}$ Ly-6C$^{-}$ MHC-II$^{+}$

796 macrophages (bottom) in small-intestinal uninf (left), PG- (middle) and PG+ (right)

797 tissue with quantification (right side) of frequency (top) and total number (bottom) of

798 neutrophils (left), monocytes (middle) and macrophages (right) in small-intestinal

799 uninf, PG- and PG+ tissue. Each circle represents one mouse. Lines represent

800 median. Pooled data from four independent experiments. Representative images of

801 four independent experiments.

802 (**e**) Fluorescently labeled whole-mount small-intestinal PG+ tissue from an *Yp*-

803 infected *Ccr2*$^{gfp/+}$ mouse. White (*Yp*-mCherry), magenta (Ly-6G-AF647), green

804 (CCR2-GFP). Scale bars = 100 μm. Representative images of two independent

805 experiments.

806 (**f**) Bacterial burdens in small-intestinal uninf, PG-, and PG+ tissue. Each circle
807 represents one mouse. Lines represent geometric mean. Pooled data from three
808 independent experiments.
809 (**g**) Cumulative bacterial burdens per intestine in PG+ tissue and PP. Each circle
810 represents one mouse. Lines represent geometric mean. Pooled data from five
811 independent experiments.
812 Mann-Whitney U test was performed for all statistical analyses. Abbreviations: *Yp*
813 (*Yersinia pseudotuberculosis*), PP (Peyer's patch), uninf (uninfected control), PG+
814 (pyogranuloma), PG- (non-granulomatous tissue), H&E (hematoxylin and eosin),
815 CFU (colony-forming units), ND (not detected), NS (not significant, $p > 0.05$).
816
817 **Figure 2. The intestinal innate inflammatory response to *Yersinia* is localized**
818 **to pyogranulomas**
819 (**a**) Principal component analysis of PG+ (pink), PG- (green), and uninf (gray)
820 samples at day 5 post-infection. Five biopsies were pooled per mouse.
821 (**b**) Heatmap of all differentially expressed genes in PG+ compared to PG- samples.
822 False discovery rate < 0.05 using Benjamini-Hochberg procedure.
823 (**c**) Heatmap of top 30 significantly upregulated genes in PG+ compared to PG-
824 samples in descending order by fold change. False discovery rate < 0.05 using
825 Benjamini-Hochberg procedure.
826 (**d**) Gene ontology analysis of top 30 upregulated genes by fold change only in PG+
827 compared to PG- samples.
828 (**e**) Gene set enrichment analysis (GSEA) of top 50 upregulated genes in *Yp*-infected
829 Peyer's patches. NES = normalized enrichment score; FDR = false discovery rate.

830 (**f**) Cytokine levels in homogenates of tissue punch biopsies were measured by
831 cytometric bead array. Lines represent group mean. Mann-Whitney U test was
832 performed for statistical analysis. NS = not significant. Data from one or two pooled
833 independent experiments.
834
835 **Figure 3. Inflammatory monocytes are required for organized pyogranuloma**
836 **formation and restriction of Yersinia within intestinal tissue**
837 (**a**) Quantification of total number of intestinal lesions at day 5 post infection. Each
838 circle represents one mouse. Lines represent median. Pooled data from four
839 independent experiments.
840 (**b**) H&E-stained paraffin-embedded longitudinal small intestinal sections from *Yp*-
841 infected mice. Scale bars = 250 μm (top) and 50 μm (bottom). Representative
842 images of two independent experiments.
843 (**c**) Histopathological scores of small intestinal tissue from uninfected and *Yp*-
844 infected mice. Each mouse was given a score between 0-4 (healthy-severe) for
845 signs of pathology. Each circle represents one mouse. Lines represent median.
846 Pooled data from two independent experiments.
847 (**d**) Bacterial burdens in small-intestinal PG- and PG+ tissue. Each circle represents
848 the mean *Yp*-CFU of 3-5 pooled punch biopsies from one mouse. Lines represent
849 geometric mean. Pooled data from six independent experiments.
850 (**e**) Total number of $CD45^+$ cells, monocytes, macrophages, and neutrophils in small
851 intestinal uninf, PG-, and PG+ tissue. Each circle represents the mean of 3-10
852 pooled punch biopsies from one mouse. Lines represent median. Pooled data from
853 five independent experiments.

854 (**f**) Fluorescently labeled whole-mount small intestinal PG+ tissue from *Yp*-infected
855 *Ccr2*$^{gfp/+}$ (top) and *Ccr2*$^{gfp/gfp}$ (bottom) mice. Scale bars = 100 μm. Representative
856 images of two independent experiments.
857 (**g**) PG+ neutrophil CD11b expression was measured by flow cytometry. Lines
858 represent median. Representative of four independent experiments.
859 (**h**) Cytokine levels in homogenates of tissue punch biopsies were measured by
860 cytometric bead array. Lines represent median. Pooled data from three independent
861 experiments.
862 Mann-Whitney U test was performed for all statistical analyses. NS = not significant.
863
864 **Figure 4. Inflammatory monocytes are required for systemic control of *Yersinia***
865 **and host survival**
866 (**a**) Bacterial burdens in indicated organs at day 5 post infection. Each circle
867 represents one mouse. Lines represent geometric mean. Pooled data from four
868 independent experiments.
869 (**b**) H&E-stained paraffin-embedded longitudinal spleen sections from WT and
870 *Ccr2*$^{gfp/gfp}$ mice. Scale bars = 500 μm (top) and 50 μm (top). Representative images
871 of two independent experiments.
872 (**c**) Histopathological scores of spleens from uninfected and *Yp*-infected mice. Each
873 mouse was given a score between 0-4 (healthy-severe) for signs of pathology. Each
874 circle represents one mouse. Lines represent median. Pooled data from two
875 independent experiments.
876 (**d**) Survival of infected WT (n=16) and *Ccr2*$^{gfp/gfp}$ (n=13) mice. Pooled data from two
877 independent experiments.

878 (**e**) Survival of infected littermate wild-type *Ccr2*$^{+/+}$ (n=20), heterozygous *Ccr2*$^{gfp/+}$
879 (n=19), and homozygous *Ccr2*$^{gfp/gfp}$ (n=15) mice. Pooled data from three independent
880 experiments.
881 Statistical analyses by (a, c) Mann-Whitney U test and (d-e) Mantel-Cox test. NS =
882 not significant.
883
884 **Figure 5. Intestinal pyogranulomas form in response to *Yersinia* virulence**
885 (**a**) Quantification of total number of intestinal lesions upon infection. Each symbol
886 represents one mouse. Lines represent median. Pooled data from 2-3 independent
887 experiments.
888 (**b**) Bacterial burdens in small-intestinal PG- (left) and PG+ (right) tissue. Each
889 symbol represents one mouse. Lines represent geometric mean. Pooled data from
890 2-3 independent experiments.
891 (**c**) Bacterial burdens in indicated organs. Each symbol represents one mouse. Lines
892 represent geometric mean. Pooled data from 2-3 independent experiments.
893 (**d**) Frequency of monocytes (left) and neutrophils (right) in small-intestinal uninf, PG-
894 and PG+ tissue. Each symbol represents one mouse. Lines represent median.
895 Pooled data from two independent experiments.
896 (**e**) Frequency of monocytes (left) and neutrophils (right) in MLN. Each symbol
897 represents one mouse. Lines represent median. Representative data from two
898 independent experiments.
899 Mann-Whitney U test was performed for all statistical analyses.
900
901 **Figure 6. *Yp* restriction by CCR2-deficient mice is restored in absence of YopH**
902 **activity**

903 (**a**) H&E-stained paraffin-embedded transverse small intestinal sections from WT
904 (top) and *Ccr2*$^{gfp/gfp}$ (bottom) mice infected with WT (left) or YopH$^{R409A}$ (right) *Yp* at
905 day 5 post infection. Scale bars = 100 μm. Representative images of two
906 independent experiments.
907 (**b**) Bacterial burdens in small-intestinal PG- and PG+ tissue at day 5 post infection.
908 Each symbol represents one mouse. Lines represent geometric mean. Pooled data
909 from two independent experiments.
910 (**c**) Bacterial burdens in indicated organs at day 5 post infection. Each symbol
911 represents one mouse. Lines represent geometric mean. Pooled data from two
912 independent experiments.
913 Mann-Whitney U test was performed for all statistical analyses. NS = not significant.
914
915 **Extended Data Figure 1. Intestinal pyogranulomas form acutely following oral**
916 ***Yersinia* infection**
917 (**a**) Quantification of total number of intestinal lesions upon *Yp* or *Ye* infection. Each
918 circle represents one mouse. Lines represent median. Pooled data from three
919 independent experiments.
920 (**b**) Frequency distribution (left) of lesions along the intestinal tract, with graphical key
921 of anatomical segments (right). Each colored bar represents the mean frequency of
922 lesions in a given segment (n = 20 mice). Only mice with >9 total pyogranulomas
923 were included. Pooled data from three independent experiments.
924 (**c**) Flow cytometry plots displaying the gating strategy employed to identify
925 eosinophils, dendritic cells, B cells and T cells in small-intestinal tissue.
926 Representative images of four independent experiments.

927 (**d**) Frequency (top) and total number (bottom) of eosinophils, dendritic cells, B cells,
928 $CD4^+$ T cells and $CD8^+$ T cells (left to right) in small-intestinal uninf, PG- and PG+
929 tissue. Each circle represents the mean of 3-10 pooled punch biopsies (ø = 2 mm)
930 from one mouse. Lines represent median. Pooled data from four independent
931 experiments.
932 Mann-Whitney U test was performed for all statistical analyses. NS = not significant.
933
934 **Extended Data Figure 2. Non-pyogranuloma tissue does not undergo a pro-**
935 **inflammatory response during intestinal *Yp* infection**
936 (**a**) Heatmap of top 30 significantly upregulated genes in PG- compared to uninfected
937 samples in descending order by fold change. False discovery rate < 0.05 using
938 Benjamini-Hochberg procedure.
939 (**b**) Gene ontology analysis of top 30 upregulated genes by fold change only in PG-
940 compared to uninfected samples. Dotted line denotes p = 0.05.
941
942 **Extended Data Figure 3. *Ccr2*$^{-/-}$ mice have increased susceptibility to oral**
943 ***Yersinia* infection.**
944 (**a**) Quantification of total number of intestinal lesions at day 3 post infection. Each
945 circle represents one mouse. Line represents median. Pooled data from two
946 independent experiments.
947 (**b**) Bacterial burdens in small intestinal PG- and PG+ tissue at day 3 post infection.
948 Each circle represents the mean *Yp*-CFU of 3-5 pooled punch biopsies from one
949 mouse. Lines represent geometric mean. Pooled data from four independent
950 experiments.

951 (**c**) Frequency of neutrophils in MLN and spleen at day 5 post infection. Each circle
952 represents the mean of 3-10 pooled punch biopsies from one mouse. Lines
953 represent median. Pooled data from two independent experiments.
954 (**d**) MLN neutrophil CD11b expression was measured by flow cytometry. Lines
955 represent median. Representative of two independent experiments.
956 (**e**) Cytokine levels in homogenates of tissue punch biopsies at day 5 post infection
957 were measured by cytometric bead array. Lines represent median. Pooled data from
958 three independent experiments.
959 (**f**) Total number of $CD4^+$ and $CD8^+$ T cells in small intestinal PG+ tissue. Each circle
960 represents the mean of 3-10 pooled punch biopsies from one mouse. Lines
961 represent median. Pooled data from 4 independent experiments.
962 (**g**) Bacterial burdens in indicated organs at day 3 post infection. Each circle
963 represents one mouse. Lines represent geometric mean. Pooled data from four
964 independent experiments.
965 (**h**) Survival of infected mice. Pooled data from two independent experiments.
966 Statistical analyses by (a-g) Mann-Whitney U test or (h) Mantel-Cox test. NS = not
967 significant.
968
969 **Extended Data Figure 4. Monocytes are dispensable for restriction of YopH**
970 **mutant *Yp***
971 (**a**) Quantification of total number of intestinal lesions upon infection. Each symbol
972 represents one mouse. Lines represent median. Pooled data from 2 independent
973 experiments.

974 (**b**) Bacterial burdens in small-intestinal PG- and PG+ tissue at day 3 post infection.
975 Each symbol represents one mouse. Lines represent geometric mean. Pooled data
976 from two independent experiments.
977 (**c**) Bacterial burdens in indicated organs at day 3 post infection. Each symbol
978 represents one mouse. Lines represent geometric mean. Pooled data from two
979 independent experiments.
980 (**d**) Survival of *Yp*-infected mice. Pooled data from two independent experiments.
981 Statistical analyses by (a-c) Mann-Whitney U test and (d) Mantel-Cox test.
982
983 **Extended Data Table 1.** Gene ontology analysis of PG+ vs PG- samples
984 **Extended Data Table 2.** Gene ontology analysis of PG- vs uninfected samples
985 **Supplementary code file**

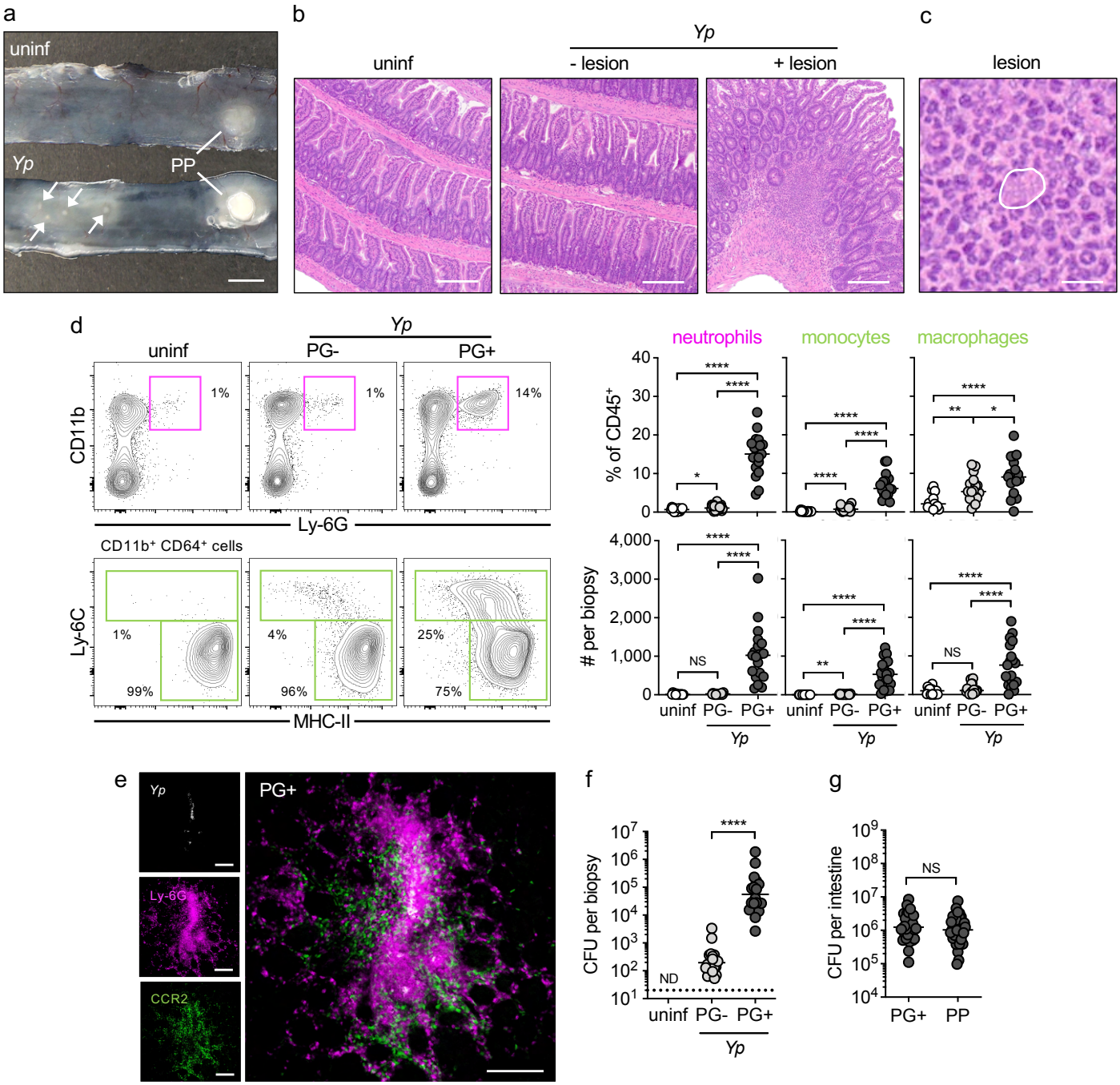


**Figure 1. Intestinal pyogranulomas form acutely following oral *Yersinia* infection**

(**a**) Longitudinal small-intestinal segments from uninf (top) and *Yp*-infected (bottom) mice with arrows depicting lesions. Scale bar = 3 mm. Representative image of >3 independent experiments.

(**b**) H&E-stained paraffin-embedded longitudinal small-intestinal sections from uninf (left) and *Yp*-infected (middle and right) mice. Scale bars = 200 µm. Representative images of three independent experiments.

(**c**) H&E-stained paraffin-embedded longitudinal small-intestinal PG+ section from a *Yp*-infected mouse depicting an encircled bacterial colony. Scale bar = 10 µm. Representative image of three independent experiments.

(**d**) Flow-cytometry plots (left side) identifying CD11b$^+$ Ly-6G$^+$ neutrophils (top), CD11b$^+$ CD64$^+$ Ly-6C$^+$ monocytes, and CD11b$^+$ CD64$^+$ Ly-6C$^-$ MHC-II$^+$ macrophages (bottom) in small-intestinal uninf (left), PG- (middle) and PG+ (right) tissue with quantification (right side) of frequency (top) and total number (bottom) of neutrophils (left), monocytes (middle) and macrophages (right) in small-intestinal uninf, PG- and PG+ tissue. Each circle represents one mouse. Lines represent median. Pooled data from four independent experiments. Representative images of four independent experiments.

(**e**) Fluorescently labeled whole-mount small-intestinal PG+ tissue from an *Yp*-infected *Ccr2$^{gfp/+}$* mouse. White (*Yp*-mCherry), magenta (Ly-6G-AF647), green (CCR2-GFP). Scale bars = 100 µm. Representative images of two independent experiments.

(**f**) Bacterial burdens in small-intestinal uninf, PG-, and PG+ tissue. Each circle represents one mouse. Lines represent geometric mean. Pooled data from three independent experiments.

(**g**) Cumulative bacterial burdens per intestine in PG+ tissue and PP. Each circle represents one mouse. Lines represent geometric mean. Pooled data from five independent experiments.

Mann-Whitney U test was performed for all statistical analyses. Abbreviations: *Yp* (*Yersinia pseudotuberculosis*), PP (Peyer's patch), uninf (uninfected control), PG+ (pyogranuloma), PG- (non-granulomatous tissue), H&E (hematoxylin and eosin), CFU (colony-forming units), ND (not detected), NS (not significant, $p > 0.05$).

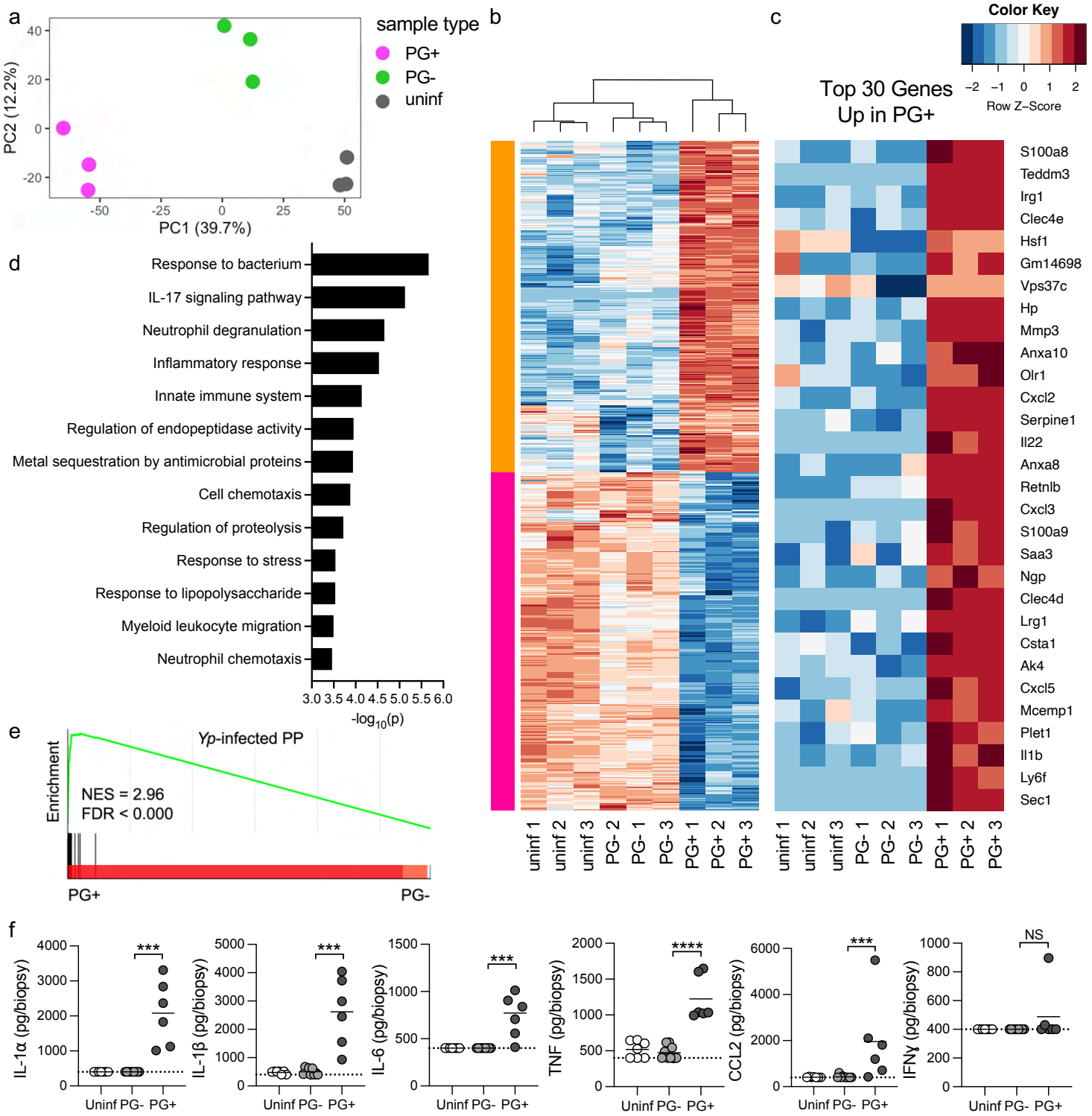


**Figure 2. The intestinal innate inflammatory response to *Yersinia* is localized to pyogranulomas**

(**a**) Principal component analysis of PG+ (pink), PG- (green), and uninf (gray) samples at day 5 post-infection. Five biopsies were pooled per mouse.

(**b**) Heatmap of all differentially expressed genes in PG+ compared to PG- samples. False discovery rate < 0.05 using Benjamini-Hochberg procedure.

(**c**) Heatmap of top 30 significantly upregulated genes in PG+ compared to PG- samples in descending order by fold change. False discovery rate < 0.05 using Benjamini-Hochberg procedure.

(**d**) Gene ontology analysis of top 30 upregulated genes by fold change only in PG+ compared to PG- samples.

(**e**) Gene set enrichment analysis (GSEA) of top 50 upregulated genes in *Yp*-infected Peyer's patches. NES = normalized enrichment score; FDR = false discovery rate.

(**f**) Cytokine levels in homogenates of tissue punch biopsies were measured by cytometric bead array. Lines represent group mean. Mann-Whitney U test was performed for statistical analysis. NS = not significant. Data from one or two pooled independent experiments.

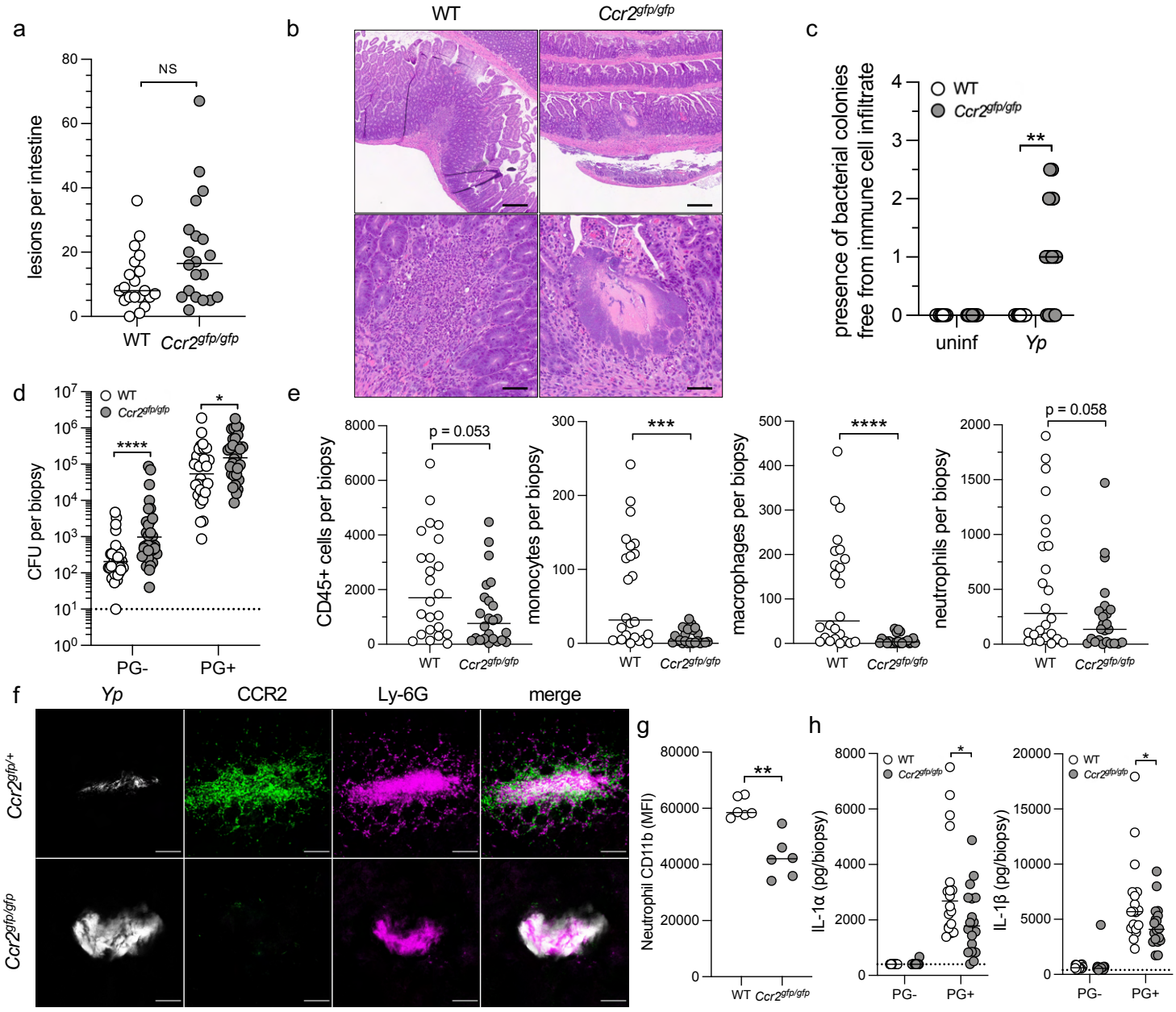


**Figure 3. Inflammatory monocytes are required for organized pyogranuloma formation and restriction of Yersinia within intestinal tissue**

(**a**) Quantification of total number of intestinal lesions at day 5 post infection. Each circle represents one mouse. Lines represent median. Pooled data from four independent experiments.

(**b**) H&E-stained paraffin-embedded longitudinal small intestinal sections from *Yp*-infected mice. Scale bars = 250 µm (top) and 50 µm (bottom). Representative images of two independent experiments.

(**c**) Histopathological scores of small intestinal tissue from uninfected and *Yp*-infected mice. Each mouse was given a score between 0-4 (healthy-severe) for signs of pathology. Each circle represents one mouse. Lines represent median. Pooled data from two independent experiments.

(**d**) Bacterial burdens in small-intestinal PG- and PG+ tissue. Each circle represents the mean *Yp*-CFU of 3-5 pooled punch biopsies from one mouse. Lines represent geometric mean. Pooled data from six independent experiments.

(**e**) Total number of CD45$^{+}$ cells, monocytes, macrophages, and neutrophils in small intestinal uninf, PG-, and PG+ tissue. Each circle represents the mean of 3-10 pooled punch biopsies from one mouse. Lines represent median. Pooled data from five independent experiments.

(**f**) Fluorescently labeled whole-mount small intestinal PG+ tissue from *Yp*-infected *Ccr2*$^{gfp/+}$ (top) and *Ccr2*$^{gfp/gfp}$ (bottom) mice. Scale bars = 100 µm. Representative images of two independent experiments.

(**g**) PG+ neutrophil CD11b expression was measured by flow cytometry. Lines represent median. Representative of four independent experiments.

(**h**) Cytokine levels in homogenates of tissue punch biopsies were measured by cytometric bead array. Lines represent median. Pooled data from three independent experiments.

Mann-Whitney U test was performed for all statistical analyses. NS = not significant.

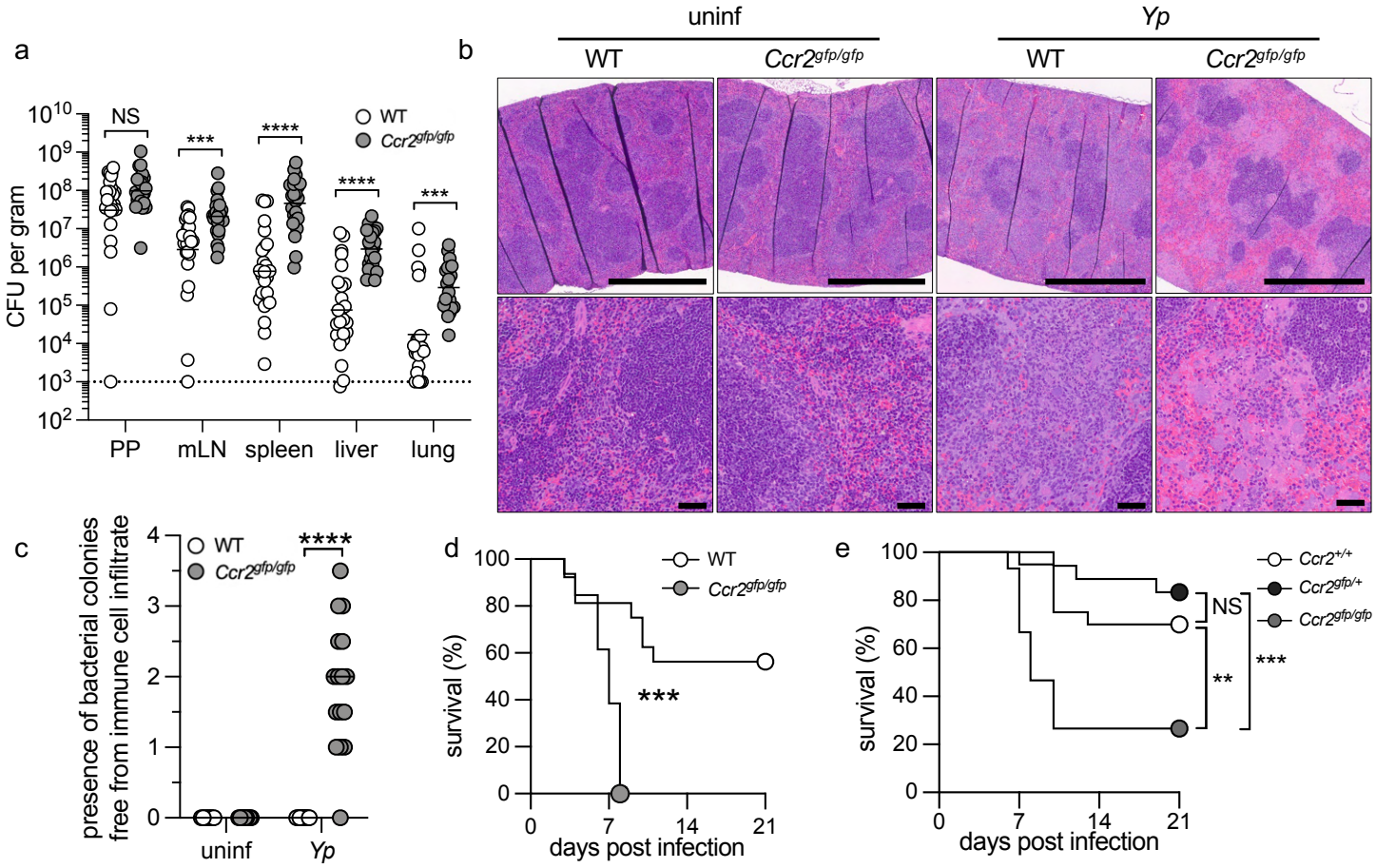


**Figure 4. Inflammatory monocytes are required for systemic control of *Yersinia* and host survival**

(**a**) Bacterial burdens in indicated organs at day 5 post infection. Each circle represents one mouse. Lines represent geometric mean. Pooled data from four independent experiments.

(**b**) H&E-stained paraffin-embedded longitudinal spleen sections from WT and *Ccr2*$^{gfp/gfp}$ mice. Scale bars = 500 µm (top) and 50 µm (top). Representative images of two independent experiments.

(**c**) Histopathological scores of spleens from uninfected and *Yp*-infected mice. Each mouse was given a score between 0-4 (healthy-severe) for signs of pathology. Each circle represents one mouse. Lines represent median. Pooled data from two independent experiments.

(**d**) Survival of infected WT (n=16) and *Ccr2*$^{gfp/gfp}$ (n=13) mice. Pooled data from two independent experiments.

(**e**) Survival of infected littermate wild-type *Ccr2*$^{+/+}$ (n=20), heterozygous *Ccr2*$^{gfp/+}$ (n=19), and homozygous *Ccr2*$^{gfp/gfp}$ (n=15) mice. Pooled data from three independent experiments.

Statistical analyses by (a, c) Mann-Whitney U test and (d-e) Mantel-Cox test. NS = not significant.

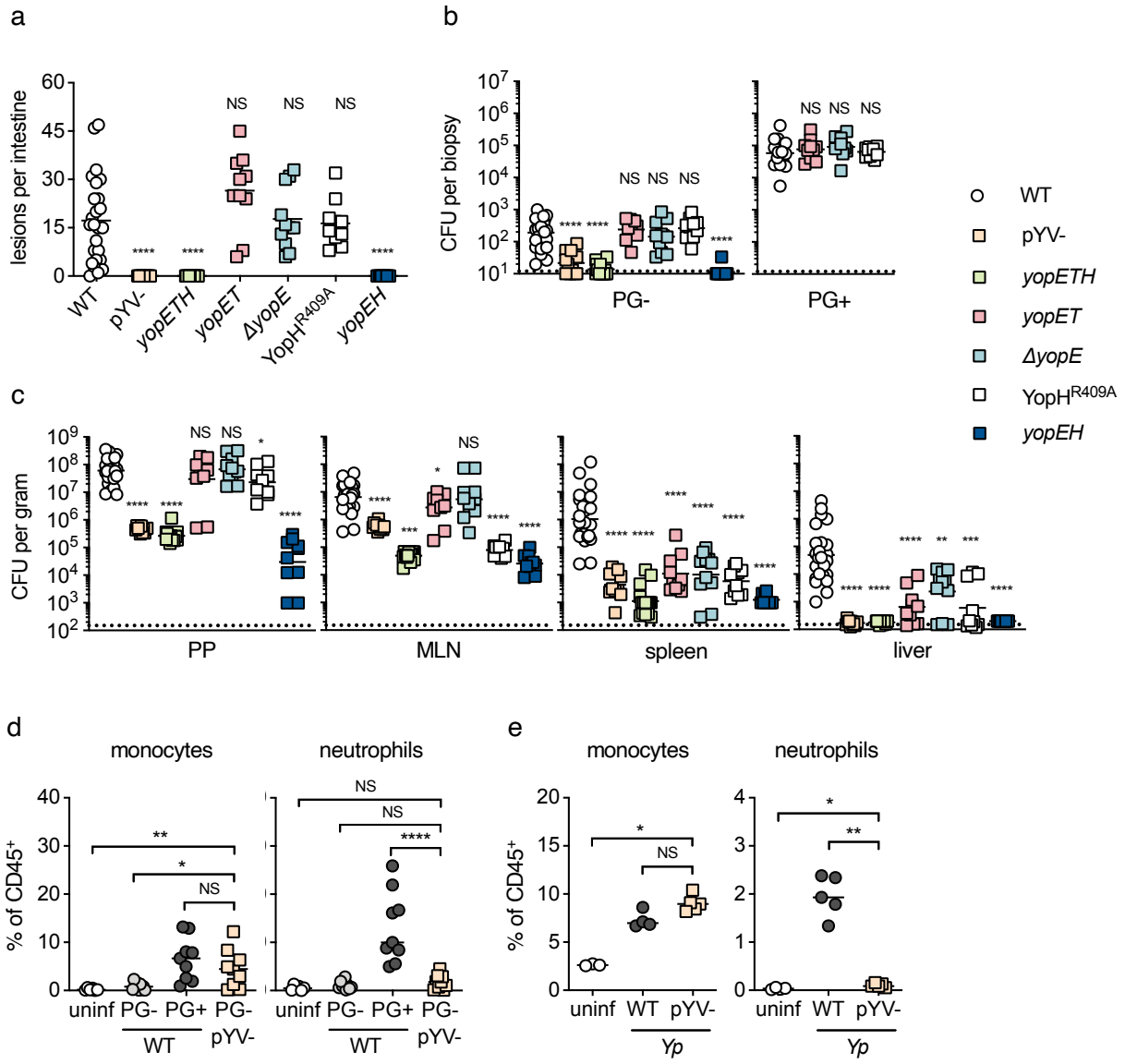


**Figure 5. Intestinal pyogranulomas form in response to *Yersinia* virulence**

(**a**) Quantification of total number of intestinal lesions upon infection. Each symbol represents one mouse. Lines represent median. Pooled data from 2-3 independent experiments.

(**b**) Bacterial burdens in small-intestinal PG- (left) and PG+ (right) tissue. Each symbol represents one mouse. Lines represent geometric mean. Pooled data from 2-3 independent experiments.

(**c**) Bacterial burdens in indicated organs. Each symbol represents one mouse. Lines represent geometric mean. Pooled data from 2-3 independent experiments.

(**d**) Frequency of monocytes (left) and neutrophils (right) in small-intestinal uninf, PG- and PG+ tissue. Each symbol represents one mouse. Lines represent median. Pooled data from two independent experiments.

(**e**) Frequency of monocytes (left) and neutrophils (right) in MLN. Each symbol represents one mouse. Lines represent median. Representative data from two independent experiments.

Mann-Whitney U test was performed for all statistical analyses.

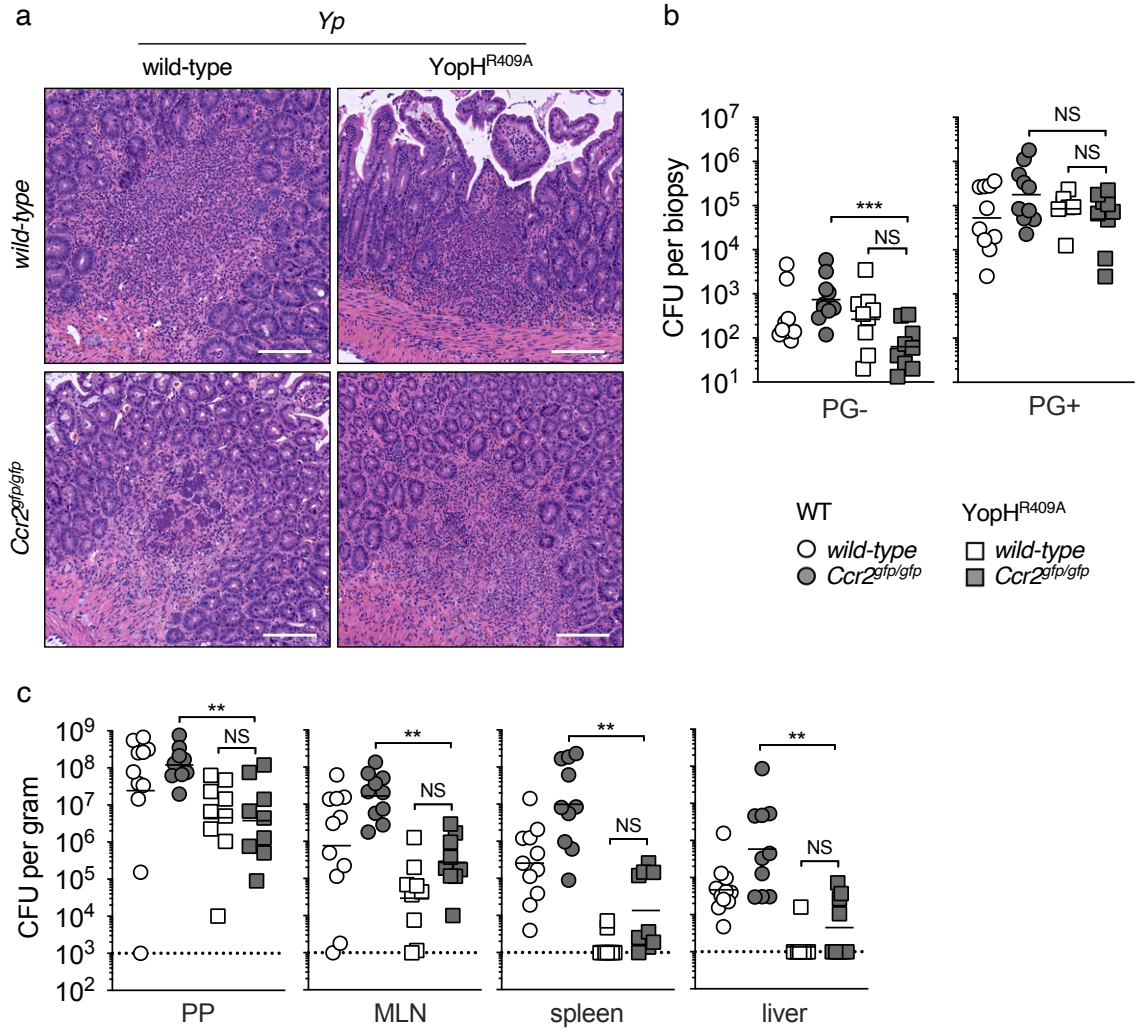


**Figure 6. *Yp* restriction by CCR2-deficient mice is restored in absence of YopH activity**

(**a**) H&E-stained paraffin-embedded transverse small intestinal sections from WT (top) and *Ccr2*$^{gfp/gfp}$ (bottom) mice infected with WT (left) or YopH$^{R409A}$ (right) *Yp* at day 5 post infection. Scale bars = 100 µm. Representative images of two independent experiments.

(**b**) Bacterial burdens in small-intestinal PG- and PG+ tissue at day 5 post infection. Each symbol represents one mouse. Lines represent geometric mean. Pooled data from two independent experiments.

(**c**) Bacterial burdens in indicated organs at day 5 post infection. Each symbol represents one mouse. Lines represent geometric mean. Pooled data from two independent experiments.

Mann-Whitney U test was performed for all statistical analyses. NS = not significant.

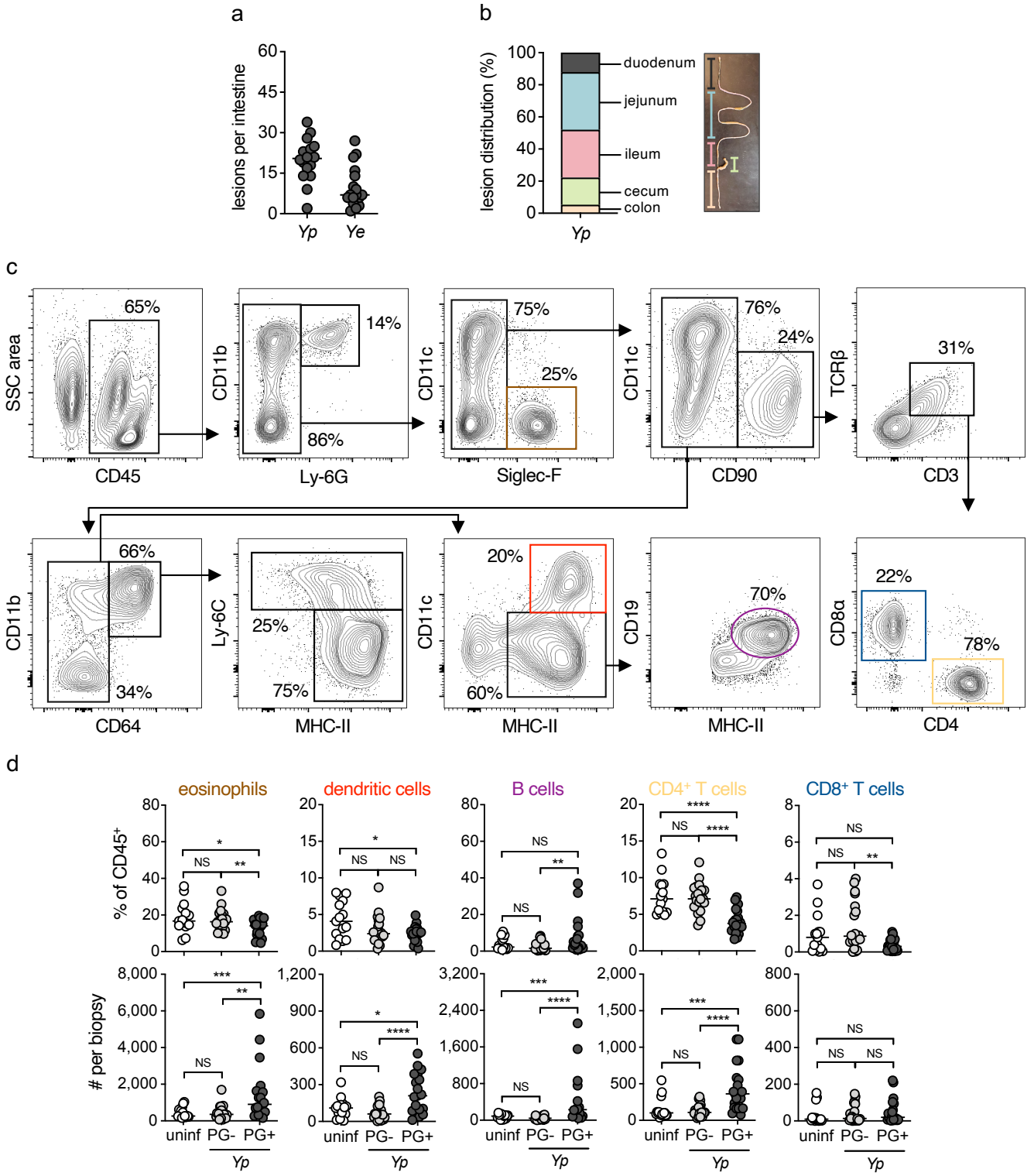


**Extended Data Figure 1. Intestinal pyogranulomas from acutely following oral *Yersinia* infection**

(**a**) Quantification of total number of intestinal lesions upon *Yp* or *Ye* infection. Each circle represents one mouse. Lines represent median. Pooled data from three independent experiments.

(**b**) Frequency distribution (left) of lesions along the intestinal tract, with graphical key of anatomical segments (right). Each colored bar represents the mean frequency of lesions in a given segment (n = 20 mice). Only mice with >9 total pyogranulomas were included. Pooled data from three independent experiments.

(**c**) Flow cytometry plots displaying the gating strategy employed to identify eosinophils, dendritic cells, B cells and T cells in small-intestinal tissue. Representative images of four independent experiments.

(**d**) Frequency (top) and total number (bottom) of eosinophils, dendritic cells, B cells, $CD4^+$ T cells and $CD8^+$ T cells (left to right) in small-intestinal uninf, PG- and PG+ tissue. Each circle represents the mean of 3-10 pooled punch biopsies (ø = 2 mm) from one mouse. Lines represent median. Pooled data from four independent experiments.

Mann-Whitney U test was performed for all statistical analyses. NS = not significant.

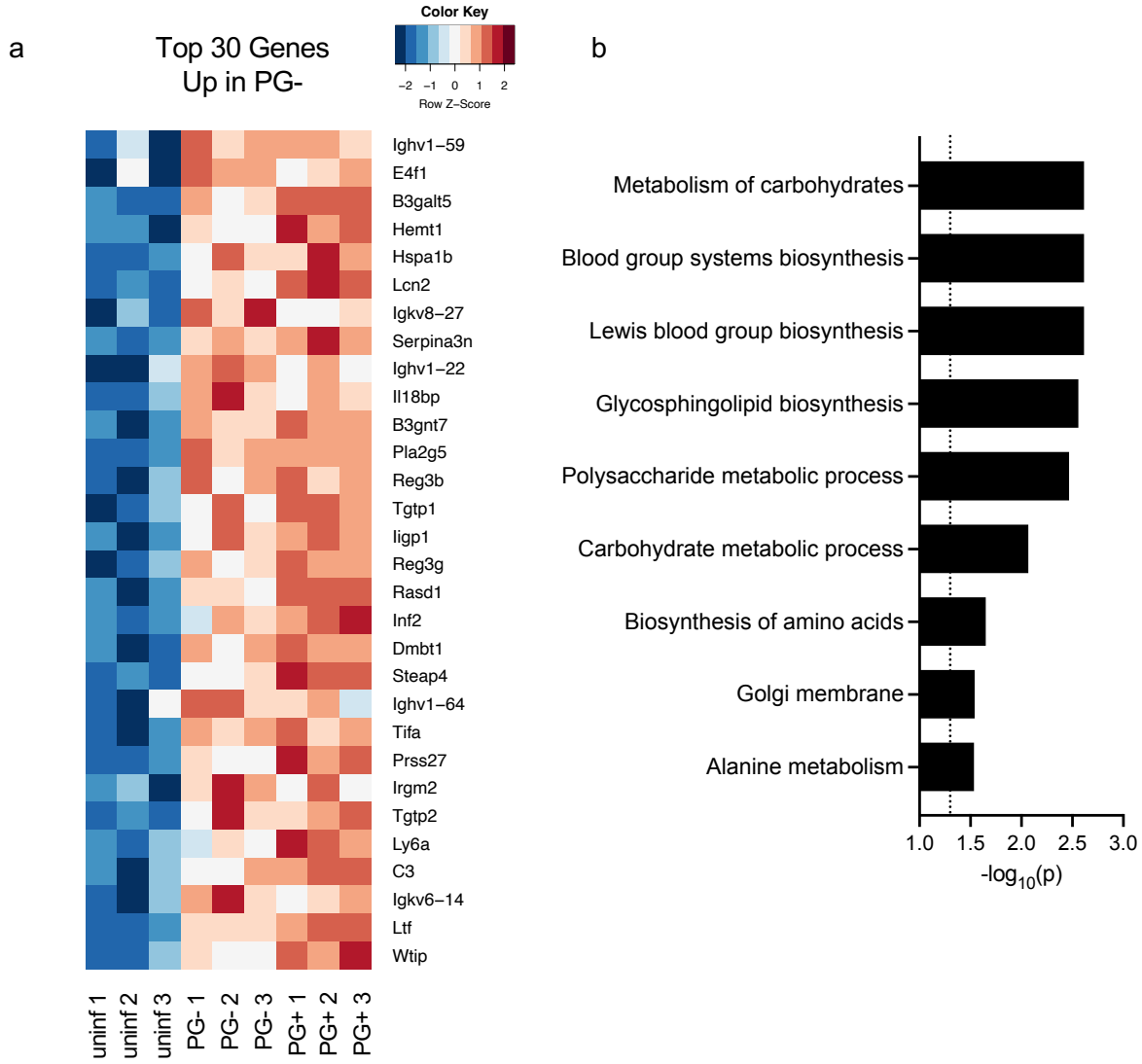


**Extended Data Figure 2. Non-pyogranuloma tissue does not undergo a pro-inflammatory response during intestinal *Yp* infection**
(**a**) Heatmap of top 30 significantly upregulated genes in PG- compared to uninfected samples in descending order by fold change. False discovery rate < 0.05 using Benjamini-Hochberg procedure.
(**b**) Gene ontology analysis of top 30 upregulated genes by fold change only in PG- compared to uninfected samples. Dotted line denotes p = 0.05.

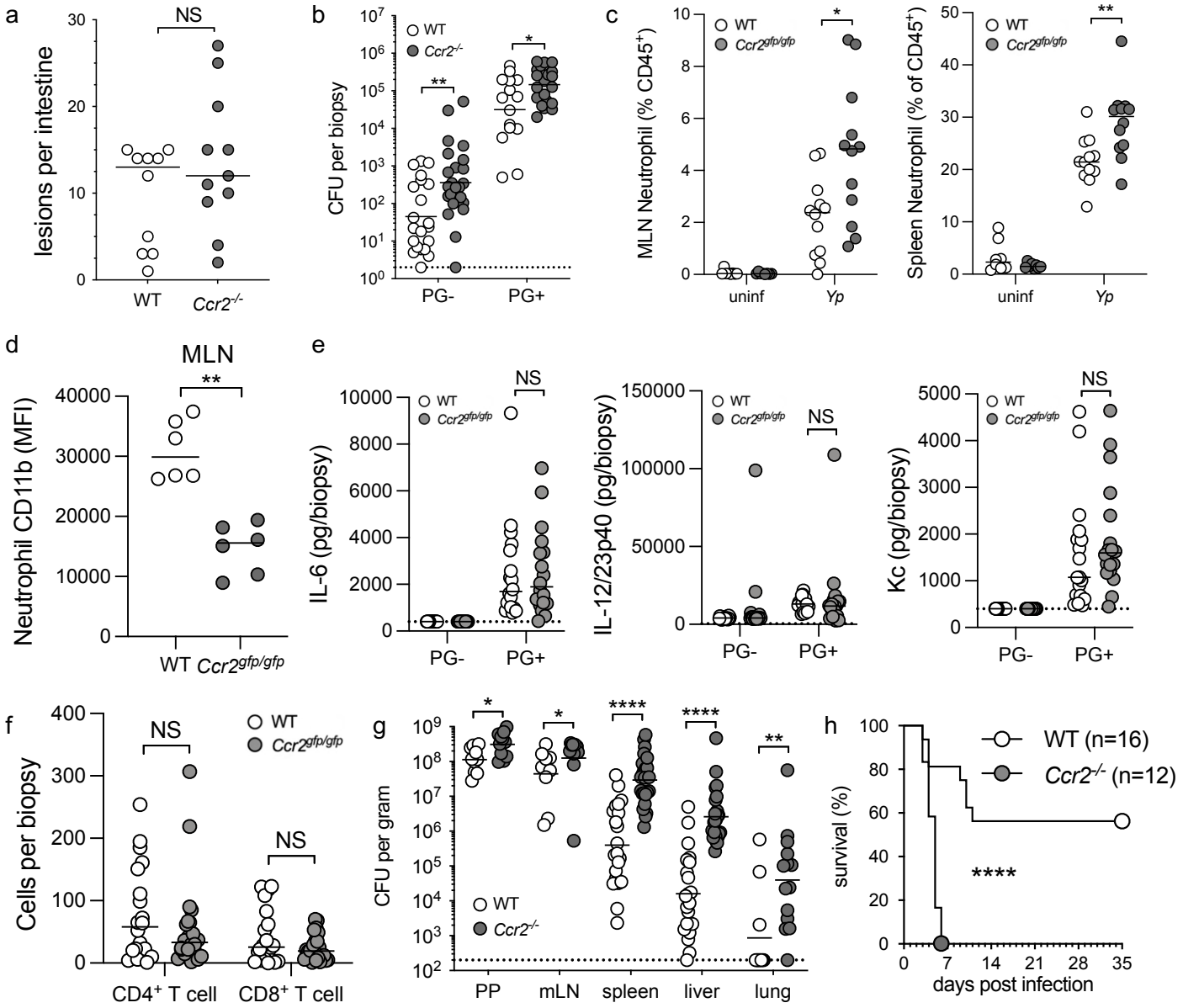


**Extended Data Figure 3. *Ccr2*$^{-/-}$ mice have increased susceptibility to oral *Yersinia* infection.**

(**a**) Quantification of total number of intestinal lesions at day 3 post infection. Each circle represents one mouse. Line represents median. Pooled data from two independent experiments.

(**b**) Bacterial burdens in small intestinal PG- and PG+ tissue at day 3 post infection. Each circle represents the mean *Yp*-CFU of 3-5 pooled punch biopsies from one mouse. Lines represent geometric mean. Pooled data from four independent experiments.

(**c**) Frequency of neutrophils in MLN and spleen at day 5 post infection. Each circle represents the mean of 3-10 pooled punch biopsies from one mouse. Lines represent median. Pooled data from two independent experiments.

(**d**) MLN neutrophil CD11b expression was measured by flow cytometry. Lines represent median. Representative of two independent experiments.

(**e**) Cytokine levels in homogenates of tissue punch biopsies at day 5 post infection were measured by cytometric bead array. Lines represent median. Pooled data from three independent experiments.

(**f**) Total number of CD4$^{+}$ and CD8$^{+}$ T cells in small intestinal PG+ tissue. Each circle represents the mean of 3-10 pooled punch biopsies from one mouse. Lines represent median. Pooled data from 4 independent experiments.

(**g**) Bacterial burdens in indicated organs at day 3 post infection. Each circle represents one mouse. Lines represent geometric mean. Pooled data from four independent experiments.

(**h**) Survival of infected mice. Pooled data from two independent experiments.

Statistical analyses by (a-g) Mann-Whitney U test or (h) Mantel-Cox test. NS = not significant.

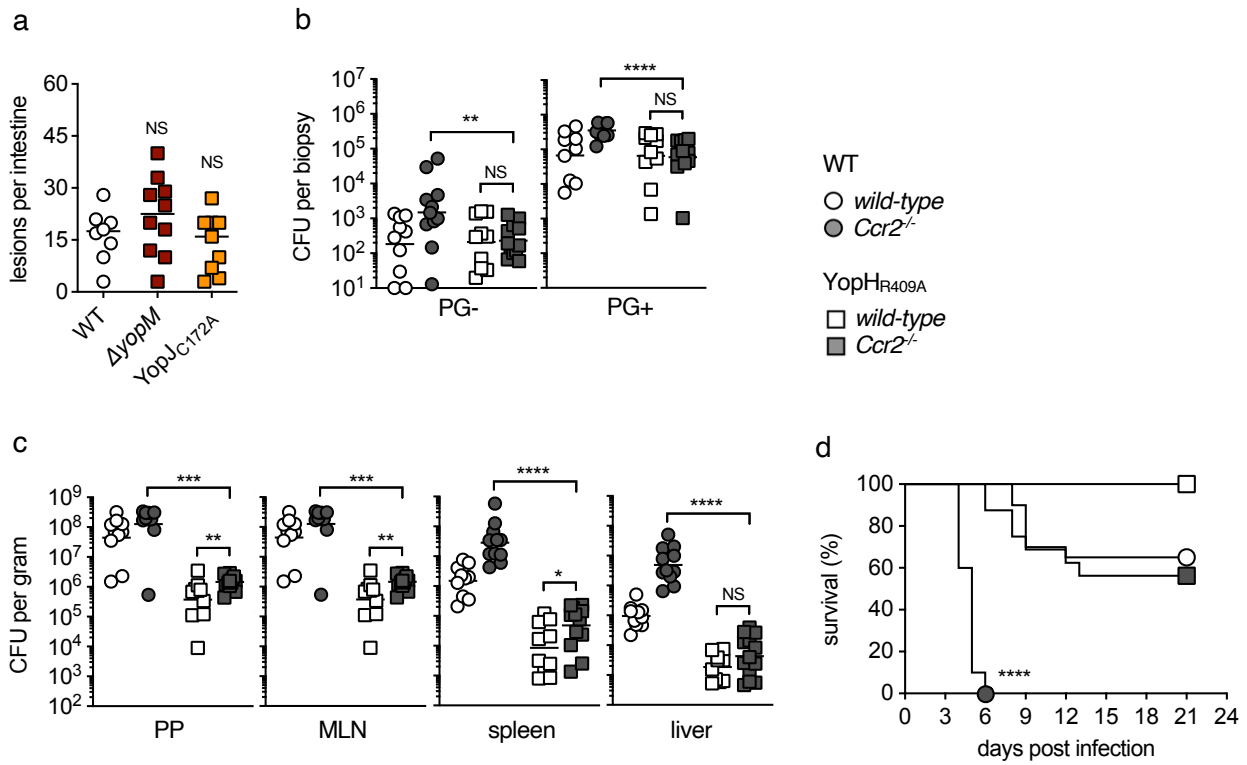


**Extended Data Figure 4. Monocytes are dispensable for restriction of YopH mutant *Yp***

(**a**) Quantification of total number of intestinal lesions upon infection. Each symbol represents one mouse. Lines represent median. Pooled data from 2 independent experiments.

(**b**) Bacterial burdens in small-intestinal PG- and PG+ tissue at day 3 post infection. Each symbol represents one mouse. Lines represent geometric mean. Pooled data from two independent experiments.

(**c**) Bacterial burdens in indicated organs at day 3 post infection. Each symbol represents one mouse. Lines represent geometric mean. Pooled data from two independent experiments.

(**d**) Survival of *Yp*-infected mice. Pooled data from two independent experiments.

Statistical analyses by (a, b) Mann-Whitney U test and (c) Mantel-Cox test.